Minireview

Machine learning and deep learning for brain tumor MRI image segmentation

Md Kamrul Hasan Khan, Wenjing Guo, Jie Liu, Fan Dong, Zoe Li, Tucker A Patterson and Huixiao Hong

National Center for Toxicological Research, U.S. Food & Drug Administration, Jefferson, AR 72079, USA
Corresponding author: Huixiao Hong. Email: huixiao.hong@fda.hhs.gov

Impact Statement

Magnetic resonance imaging (MRI) is widely used for brain tumor diagnosis. Accurately segmenting MRI images is crucial in clinical practices. Machine learning and deep learning techniques have been extensively explored for automation of brain tumor MRI image segmentation. A systematic review of machine learning and deep learning methods for brain tumor MRI image segmentation could facilitate and promote applications of machine learning and deep learning for brain tumor MRI image segmentation in clinical practices. This review article summarizes machine learning and deep learning algorithms and architectures that have been explored for brain tumor image segmentation. The technical details, advantages, and limitations of each method are discussed to help readers better understanding of the methods and utilizing these methods in clinical applications.

Abstract

Brain tumors are often fatal. Therefore, accurate brain tumor image segmentation is critical for the diagnosis, treatment, and monitoring of patients with these tumors. Magnetic resonance imaging (MRI) is a commonly used imaging technique for capturing brain images. Both machine learning and deep learning techniques are popular in analyzing MRI images. This article reviews some commonly used machine learning and deep learning techniques for brain tumor MRI image segmentation. The limitations and advantages of the reviewed machine learning and deep learning methods are discussed. Even though each of these methods has a well-established status in their individual domains, the combination of two or more techniques is currently an emerging trend.

Keywords: Machine learning, deep learning, brain, tumor, image segmentation, magnetic resonance imaging

Experimental Biology and Medicine **2023; 248: 1974–1992. DOI: 10.1177/15353702231214259**

Introduction

A brain tumor is an abnormal cell growth in the brain or in the tissues surrounding the brain. It can be benign or malignant. A benign brain tumor is homogeneous in structure without cancerous cells. Alternately, the structure of a malignant brain tumor is heterogeneous and contains cancer tissues. Gliomas and meningiomas are a class of benign tumors (low-grade tumors) that grow slowly and look similar to normal brain cells, whereas glioblastomas and astrocytomas, which tend to grow very quickly, are examples of malignant tumors (high-grade tumors).[1]

Brain tumors may be life-threatening so early diagnosis plays a critical role in treatment. A variety of diagnostic imaging techniques, including MRI, computed tomography, positron emission tomography, and single-photon emission computed tomography, are currently in use to obtain useful information on size, location, shape, and metabolism of brain tumors.[2] Among these techniques, MRI is frequently used for diagnosis of brain tumor because it is a non-invasive imaging technique, has high resolution to discern different brain tissues,[3] and does not involve exposure to ionizing radiation.[4]

MRI can detect various types of brain tumors, such as malignant and benign tumors. MRI images can be used to obtain precise anatomical details, to differentiate between different types of brain tissues, and to identify tumor location, size, and boundaries. MRI can also be used to determine the characteristics and nature of brain tumors, to differentiate between solid tumors, cysts, and areas of necrosis, and to provide information about tumor vascularity for treatment planning. The crucial task in brain tumor MRI image analysis is to identify and delineate the regions of interest in the brain before the image segmentation. Segmentation of brain tumor MRI images is the process of separating MRI scans into distinct regions or structures for analysis and interpretation,

ISSN 1535-3702

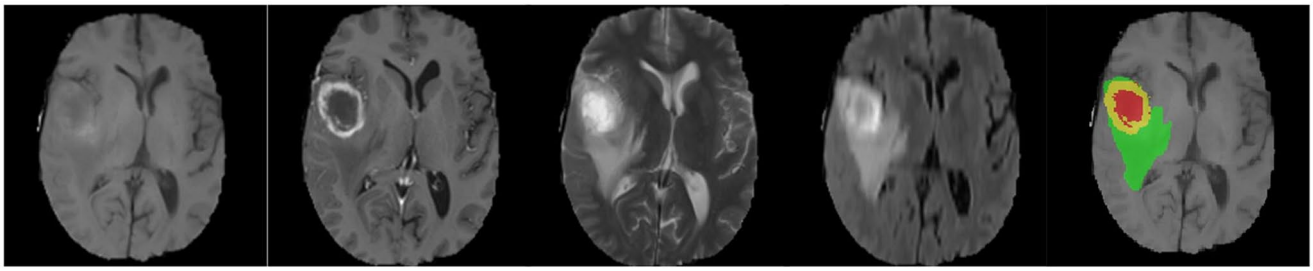

Figure 1. Example of data from BraTS 2018 training data set. From left to right: T1-weighted image, contrast-enhanced T1-weighted image, T2-weighted image, FLAIR image, and the ground truth where red, yellow, and green represent tumor core, enhanced tumor, and edema regions, respectively.[9]

such as distinguishing different brain tissues (e.g. white matter, gray matter, and cerebrospinal fluid).[5] MRI image segmentation aims to accurately identify and separate different anatomical structures or pathologies within the scanned image. The location and extent of the tumor regions can be estimated through segmentation. The borders of glioblastomas are often blurred and difficult to differentiate from healthy tissue due to their infiltrative nature. To address this issue, multiple MRI modalities, such as T1-weighted, T2-weighted, contrast-enhanced, and fluid attenuation inversion recovery (FLAIR) images, that give additional information about brain tumors, are routinely used.[6,7] Figure 1 presents an axial slice of the four sequences of MRI modalities and the ground truth. Generally, T1-weighted images separate brain tissues (particularly white matter and gray matter), T2-weighted images delineate the edema regions that produce bright signals on the image, FLAIR images are the best for separating edema regions from the cerebrospinal fluid, and contrast-enhanced images distinguish the tumor border easily because gadolinium ions (the accumulated contrast agent) in the active cells of the tumor tissue creates a bright signal. Moreover, contrast-enhanced images separate necrotic cells from the active cell region because necrotic cells do not interact with gadolinium ions and can be noticed by the low intense part of the tumor core.[2,8]

The methods for segmenting brain tumor MRI images are broadly categorized into two types: manual and automated segmentation. Traditionally, the segmentation of MRI images is performed manually. Manual segmentation involves human experts manually outlining or labeling the desired structures. Thus, it is subjective and time-consuming. Moreover, many MRI images are generated in current clinical practices for diagnosing brain tumors, and it is almost impossible to conduct manual segmentation for such large amounts of images in a reasonable time. Therefore, automated segmentation has been widely used. Automated segmentation utilizes computational algorithms and machine learning techniques to automatically identify and delineate the regions of interest. However, the manual segmentation results are regarded as the ground truth for developing and evaluating automated segmentation methods, including machine learning and deep learning methods.

There are various approaches to automated brain tumor MRI image segmentation, including thresholding, region-, edge-, machine learning-, and deep learning-based methods. Thresholding method involves setting intensity thresholds to separate different tissues based on their pixel intensities. Region-based methods use statistical or mathematical models to identify regions based on homogeneity or similarity criteria. Edge-based methods focus on detecting boundaries or edges between different structures using gradient information or edge detection algorithms. Machine learning-based approaches leverage supervised or unsupervised machine learning algorithms to learn from training data and automatically segment brain tumor MRI images. Deep neural networks such as convolutional neural network (CNN) and U-Net have shown great success in brain tumor MRI image segmentation by learning hierarchical features and capturing complex patterns.

Machine learning techniques, specifically deep learning techniques, are commonly adopted for brain tumor MRI image segmentation. Many machine learning and deep learning models have been developed for various tasks in brain tumor MRI image segmentation. Therefore, this article reviews some frequently used machine learning and deep learning techniques in brain tumor MRI image segmentation and discusses factors that impact performance of machine learning and deep learning models for MRI image segmentation.

Data sets used in machine learning and deep learning for brain tumor MRI image segmentation

Some data sets have been used for developing machine learning and deep learning models for brain tumor MRI image segmentation. Below are some frequently used data sets.

Brain Tumor Segmentation Challenge (BraTS): The BraTS data set[9] is published by the University of Pennsylvania's Center for Biomedical Image Computing & Analytics and is frequently used as benchmarking data for brain tumor MRI image segmentation. This data set is generated using different clinical protocols and scanners in multiple institutions. It includes multi-modal MRI scans (T1-weighted, T2-weighted, T1-weighted contrast-enhanced, and FLAIR) of patients with gliomas. This data set contains ground truth segmentations of various tumor subregions determined by radiologists, including tumor core, whole tumor, and enhancing tumor. Table 1 summarizes the BraTS data sets.

The Cancer Imaging Archive (TCIA): TCIA (http://www.cancerimagingarchive.net/) hosts a variety of publicly

Table 1. Number of patients in the BraTS challenge data sets.

Year	Training set	Validation set	Testing set
2012	30	–	15
2013	30	–	10
2014	200	–	38
2015	274	–	53
2016	274	–	191
2017	285	46	146
2018	285	66	191
2019	335	125	166
2020	369	125	166
2021	1251	219	570

available brain tumor MRI data sets, including the TCGA-LGG and TCGA-GBM collections. These data sets consist of pre-operative MRI scans, including T1-weighted, T2-weighted, and FLAIR, along with manual tumor segmentations.

The Brain Web data set (http://brainweb.bic.mni.mcgill.ca/cgi/brainweb1): It contains simulated three-dimensional (3D) normal brain MRI image data generated from three modalities (proton density-weighted, T1-weighted, and T2-weighted) and can be potentially used as ground truth. This data set included multiple slice thicknesses, noise levels, and intensity nonuniformity levels.

The Internet Brain Segmentation Repository (IBSR): IBSR (https://www.nitrc.org/projects/ibsr) is a repository developed by Massachusetts General Hospital. It provides expert manual segmentation of various anatomical structures along with MRI images that can used as a standardized mechanism for evaluation of machine learning and deep learning algorithms in terms of shape complexity, contrast-to-noise ratio, sensitivity to signal-to-noise ratio, degree of partial volume effect, and so on. However, IBSR does not contain segmentation of tumors.

It is worth noting that some data sets might require registration or approval from the host institutions. Researchers often combine these data sets with additional preprocessing techniques, data augmentation, or cross-validation strategies to enhance the performance and generalizability of their models.

Performance evaluation methods for MRI image segmentation

Evaluating the segmentation model performance is important in model development. To assess the performance of machine learning algorithms for MRI image segmentation, several metrics can be employed. For binary image segmentation, such as brain tumor or non-tumor regions, model predictions are compared against the ground truth label annotated by radiologists to determine true positives (TPs) that refer to actual positives correctly predicted, false positives (FPs) that are actual negatives incorrectly predicted, true negatives (TNs) that represent actual negatives correctly predicted, and false negatives (FNs) that denote actual positives incorrectly predicted. Then, various performance metrics can be calculated based on the comparison results.

Dice score (dice similarity coefficient): Dice score estimates the agreement between ground truth and predicted segmentation and is computed using the intersection and union of ground truth and predicted segmentation by equation (1)

$$Dice\left(\Omega_t,\Omega_p\right)=2\frac{\left|\Omega_t\bigcap\Omega_p\right|}{\left|\Omega_t\right|+\left|\Omega_p\right|} \tag{1}$$

where Ω_t and Ω_p are ground truth segmentation of a target image and predicted segmentation, respectively. In binary segmentation, dice score is derived from the comparison results by equation (2)

$$\mathrm{Dice}\left(\Omega_t,\Omega_p\right)=\frac{2*\mathrm{TP}}{2*\mathrm{TP}+\mathrm{FP}+\mathrm{FN}} \tag{2}$$

A higher dice score (ranging from 0 to 1) indicates better segmentation accuracy. Conceptually, dice score can be considered as a special case of Cohen's kappa coefficient, which is a commonly used statistic in reliability analysis for cases where background voxels are much more than target voxels.

Intersection over union: Intersection over union is another segmentation performance metric that quantifies the overlap between ground true and predicted areas. It is calculated by dividing the intersection by the union of the two masks. Its value is between 0 and 1. A higher value indicates a better segmentation performance. For binary segmentation, it can be computed from the comparison results by equation (3). However, this metric can be misleading when assessing performance on imbalanced data sets

$$\text{Intersection over union}=\frac{\mathrm{TP}}{\mathrm{TP}+\mathrm{FP}+\mathrm{FN}+TN} \tag{3}$$

Precision (positive predictive value): Precision is the percentage of positive predictions that are TPs and can be calculated by equation (4)

$$\mathrm{Precision}=\frac{\mathrm{TP}}{\mathrm{TP}+\mathrm{FP}} \tag{4}$$

Recall (sensitivity): Recall is the percentage of TPs that are correctly predicted and can be calculated by equation (5)

$$\mathrm{Recall}=\frac{\mathrm{TP}}{\mathrm{TP}+\mathrm{FN}} \tag{5}$$

F1-score: The *F*1-score combines recall and precision, resulting a single metrics that balances both measures and can be calculated by equation (6). *F*1-score is the harmonic mean of recall and precision and is a better overall performance measure than accuracy

$$F1-\mathrm{score}=2*\frac{\mathrm{Precision}*\mathrm{recall}}{\mathrm{Precision}+\mathrm{recall}} \tag{6}$$

Specificity (TN rate): Specificity of a test determines the ability to identify the negative cases correctly. A highly specific test implies there are few negative cases that are not correctly classified. It can be calculated by equation (7)

$$\mathrm{Specificity}=\frac{\mathrm{TN}}{\mathrm{TN}+\mathrm{FP}} \tag{7}$$

Accuracy: Accuracy measures the overall correctness of the segmentation by calculating the ratio of the pixels correctly predicted to all pixels in an image. It can be calculated using equation (8). However, accuracy can be misleading when assessing performance on imbalanced data sets, where the majority of pixels belong to one class.

$$\text{Accuracy} = \frac{\text{TP} + \text{TN}}{\text{TP} + \text{FP} + \text{FN} + \text{TN}} \tag{8}$$

Balanced Accuracy: Balanced accuracy is more appropriate when dealing with imbalanced data sets, especially when one class significantly outnumbers the other. It is calculated by equation (9), which takes the average of sensitivity and specificity

$$\text{Balanced Accuracy} = \frac{\text{Sensitivity} + \text{Specificity}}{2} \tag{9}$$

Receiver operating characteristic curve and area under the ROC curve: Receiver-operating characteristic (ROC) curve is a graphical chart that illustrates the trade-off between sensitivity and specificity by varying the classification threshold. Area under the curve (AUC) summarizes the overall performance of the model using an aggregate measure of performance across various threshold values. This performance evaluation approach is commonly used when dealing with probabilistic or confidence-based segmentation models.

Cross-validation is a method that helps assess the generalization ability of an image segmentation model. In a cross-validation, the data set is split into multiple subsets and the model is trained on some subsets and tested on the remaining subsets to assess its performance. Common cross-validation practices include k-fold cross-validation and leave-one-out cross-validation. It is important to choose evaluation methods that are appropriate for the specific segmentation task and data set characteristics. It is good practice to use a combination of multiple metrics to obtain a comprehensive understanding of performance of brain tumor MRI image segmentation models.

Machine learning for brain tumor image segmentation

Machine learning is the core component of artificial intelligence and has been extensively explored in every fields, including biological, toxicological, and medical research.[10–15] Machine learning techniques are extensively utilized in the field of MRI image segmentation because of their capacity to automatically learn and extract meaningful features from data. Here, we summarize machine learning approaches used for MRI image segmentation and discuss some widely used methods, such as mixture model and support vector machine (SVM).

Unsupervised machine learning

Unsupervised machine learning techniques are applied when labeled training data are not available. These methods aim to discover patterns, clusters, or structures in the data without prior knowledge. Unsupervised learning algorithms, such as k-means clustering,[16,17] fuzzy c-means clustering,[18–21] optimal fuzzy clustering,[22] and sparse subspace clustering[23] have been employed for unsupervised segmentation of MRI images. Next, we discuss the popular unsupervised machine learning, mixture models, in brain tumor MRI image segmentation.

Although voxels from different tissue regions may have different probability distributions, it is assumed that voxels from the same tissue region follow the same probability distribution. Therefore, the probability distribution for any voxel can be viewed as a mixture model, a weighted summation of parametric probability distributions or mixture components. For this reason, the mixture model is a popular unsupervised machine learning method for brain MRI images segmentation. Most literature considers finite mixture models where the data points are assumed to come from a mixture of some distributions. Several mixture models, such as Student's *t*-mixture models and Gaussian mixture models (GMMs) are used for segmenting brain tumor MRI images. However, GMM is the commonly used mixture model for brain tumor image segmentation. Wang *et al*.[24] proposed a method for automatically segmenting brain tumor MRI images, which relies on a normalized Gaussian Bayesian classifier and a 3D fluid vector flow algorithm. In this method, a Gaussian Bayesian classifier was developed to generate a Gaussian Bayesian brain map from brain MRI images. The brain map was then processed to initialize the 3D fluid vector flow algorithm for segmenting the brain tumor. However, validations found this method works well for some data sets but not for others.

Chaddad[25] extracted glioblastoma features from MRI scans using GMMs, principal component analysis (PCA), and wavelet. The extracted features using those three methods were then used to develop discriminative models for distinguishing tumor areas and normal areas by machine learning algorithms naive Bayes, SVM, and probabilistic neural network. Comparative analysis on the performance of those modes found that the models based on features generated from GMMs performed the best, demonstrating that the GMM is an accurate segmentation method to extract informative features from brain tumor MRI images. Other modified GMMs, such as the local variational GMM[26] and gray-level co-occurrence matrix model,[27] were also proposed and validated, demonstrating that GMMs and modified GMMs not only efficiently segment MRI images but also offer an accurate representation of the distribution of critical brain cells.

Student's *t*-distribution and Gaussian distribution are probability distributions frequently used in statistical inference and hypothesis testing. Student's *t*-distribution was used as an alternative to Gaussian distribution in the mixture model. Relative to the Gaussian distribution, *t*-distribution exhibits a flatter and more spread-out shape, is more robust to outliers due to its bell-shaped curve with heavier tails and is more suitable for small sample size. A Student's *t*-mixture model was used to iteratively segment multiple sclerosis in FLAIR images.[28] Validation of this method using the clinical MRI images from the 2015 longitudinal multiple sclerosis lesion segmentation challenge indicated that the *t*-distribution model is a viable alternative to Gaussian distribution in mixture models for MRI image segmentation, especially when sample size is small.

Table 2. Performance of machine learning models.

Algorithm	Data set	Performance metrics	Performance		
			Whole tumor	Tumor core	Enhanced tumor
Decision tree[33]	BraTS 2017	*F*-score	0.98	0.75	0.69
Random forest[34]	BraTS 2018	Dice score	0.72	0.70	0.68
Random forest[35]	BraTS 2018	Three-class accuracy	0.61		
SVM (quadratic)[37]	46 MRI (training) & 50 MRI (test)	Accuracy[a]	0.84 (normal versus abnormal)		
Proximal SVM[39]	IBSR 1.0[b]	Accuracy[a]	0.92 (normal versus abnormal)		
Twin SVM (linear kernel)[40]	Hapetitis[c]	Accuracy[a]	0.81		
Twin SVM (RBF kernel)[40]	Hapetitis[c]	Accuracy[a]	0.83		
ResNet-SVM[41]	260 MRI (training) and 112 MRI (test)	Accuracy[a]	0.89		
SVM (linear kernel)[42]	BraTS 2015	Accuracy[a]	0.94		
SVM (RBF kernel)[42]	BraTS 2015	Accuracy[a]	0.98		

SVM: support vector machine; MRI: magnetic resonance imaging; IBSR: Internet Brain Segmentation Repository.
[a]Two-class (normal versus abnormal) classification accuracy.
[b]Internet Brain Segmentation Repository (IBSR) 1.0 from the Massachusetts General Hospital has 20T1-weighted volumetric images.
[c]Data set is from the Machine Learning Repository, University of California, Irvine (http://www.ics.uci.edu/~mlearn/MLRepository.html).

Student's *t*-mixture models and GMMs assume the anatomical label of a voxel is independent of the label of other voxels, thus discard the spatial association among the voxels, making them sensitive to noise. Therefore, several methods were proposed to integrate spatial information into conventional GMM, with the prior probability of each pixel being determined through the utilization of information from neighboring pixels.[29–32] For example, Ji *et al*.[29] introduced a fuzzy local GMM method that includes spatial constraints within local GMMs for automated brain tumor MRI image segmentation. Validation of this algorithm on some synthetic and clinical MRI data demonstrated that it improved accuracy in brain tumor MRI image segmentation since it can overcome the difficulties associated with noise and low contrast for general GMM. An extension of GMM was proposed to include spatial information within conventional GMM.[30] The extended GMM uses both intensities and spatial attributes of the pixels for inferring prior probabilities, and validations on both simulated and true brain MR images showed efficacy of brain tumor MRI image segmentation. A hybrid GMM with a spatially variant finite mixture model was proposed to mitigate the sensitivity to noise of GMM by taking account of the spatial dependencies between pixels using a Markov random field model.[31] Testing on brain tumor MRI image segmentation showed that this hybrid model is more accurate in separating region of interest, such as tumor from noise than GMMs. Incorporating the spatial association, Chen *et al*.[32] introduced an enhanced hierarchical fuzzy c-means approach to segment brain MRI images, employing the anisotropic multivariate Student *t*-distribution.

Supervised machine learning

In supervised machine learning, a training data set consisting of MRI images and corresponding manually segmented labels is used to train a machine learning model. Various algorithms, such as decision tree,[33] random forests,[34,35] and SVM[36–41] can be utilized. Machine learning models learn to classify and segment different regions using the features derived from the input images. Table 2 summarizes the machine learning models reported for MRI image segmentation or classification.

SVM is a supervised machine learning technique. For binary data, it classifies two classes by creating a hyperplane either within the original input space (linear classifiers) or within a higher dimensional space mapped from the original input data (non-linear classifiers) as illustrated with the black line for two-dimensional (2D) case in Figure 2. This hyperplane maximizes the distances to the nearest data points of both sides.[36] Different kernel functions can be applied in SVM. Therefore, both linearly separable and not linearly separable data can be studied using SVM with different kernels.[37] Bahadure *et al*.[1] and Ayachi and Ben Amor[36] classified normal and tumor tissues based on the MRI images using SVM.

The proximal support vector machine (PSVM), a much simpler classification algorithm, was proposed. PSVM classifies data points based on the proximity to the parallel planes which stretch as much as possible,[38] as illustrated by the red and blue lines for 2D case in Figure 2. PSVM is computationally efficient with similar performance as compared to standard SVM. Based on segmentation results, PSVM showed 92% accuracy in detecting the tumor from an MRI brain image compared to the standard SVM with 82% accuracy.[22] First, the features were extracted utilizing histogram equalization to enhance the segmentation accuracy. The MRI brain image was then segmented using self-organizing map (SOM) clustering. The resulting images from the segmentation were then fed into the PSVM classifier. Subsequently, feature extraction and selection were applied, involving the use of the gray-level co-occurrence matrix, to prevent the occurrence of misclustered regions and PCA was used to enhance classifier accuracy.

Khemchandani and Chandra[40] introduced another variant of SVM for binary classification named twin SVM that generates two nonparallel planes in a manner where each plane is in close proximity to one class while maximizing its separation from the other. The fundamental difference between SVM and twin SVM is twin SVM solves two simpler quadratic programming problems (QPPs), while standard

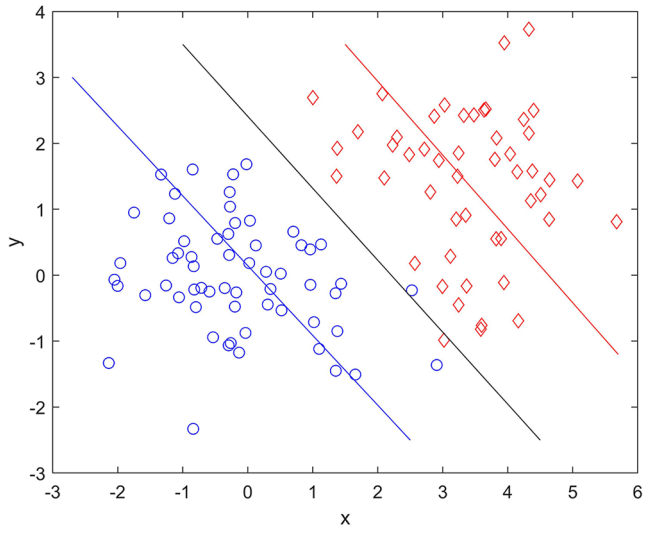

Figure 2. Illustration of the concept of two-class SVM and PSVM for a two-dimensional case. The blue circles represent samples of one class and the red diamonds are samples of another class with two independent variables *x* and *y*. SVM identifies the black line (hyperplane in high dimension) that has maximum margins to separate the two classes of samples. PSVM find the blue and red lines (hyperplanes in high dimension) in the corresponding classes of samples so that the most samples are assigned to correct classes by comparing their distances to both lines (the shorter distances win).

SVM solves one complex QPP including all observations in the constraints. In twin SVM, one class' patterns were used to set the constraints for QPP of another class. Hence, twin SVM is computationally faster. Once Otsu thresholding is applied for segmentation, the subsequent steps include employing the discrete wavelet transform for feature extraction and utilizing PCA for feature reduction. Vadhnani and Singh[42] applied SVM and its different variants in the classification phase. Comparative performance analysis revealed that twin SVM exhibited superior performance to other classifiers.

Deep learning methods

Deep learning is a mixed learning approach. It first progressively learns higher-level features from a provided data using multiple layers and then learns objects in learning using the deepest layer. Due to the increase in learning data and computational power, deep learning has gained attentions everywhere including scientific research.[43–45] Deep learning techniques have become popular for brain tumor image segmentation because of their automated feature learning capability from raw data and make accurate predictions without the need for manual feature engineering. The subsequent sections delve into several commonly employed deep learning techniques.

Convolutional neural network. Recently, CNNs have gained popularity in image analysis for their inherent capability of automatic intricate feature extractions directly from the data itself. CNNs comprise a sequence of convolutional and pooling layers that are organized sequentially. In the convolutional layer, a filter is applied to the input image to extract features that are passed through an activation function. Filter size is specified by the user. The resulting features are then directed to a pooling layer to reduce spatial dimensions. The final output of the convolutional and pooling layers sequence is then passed through a fully connected layer from which the final predictions are made.

An automated segmentation technique utilizing CNN was developed employing small kernels.[46] To achieve a deep architecture that prevents overfitting, small 3×3convolution filters were used. Using very small kernels show effectiveness in increasing convolutional network depth to improve accuracy in the recognition of large-scale images.[47] MRI image pre-processing, such as intensity normalization [48] was not commonly applied in CNN-based segmentation. Although uncommon in CNN-based segmentation methods, image pre-processing was found to be highly effective for segmenting brain tumor images when combined with data augmentation. The assessment of this CNN-based method, conducted on the BraTS 2013 and BraTS 2015 data sets, demonstrated its remarkable accuracy, effectiveness, and reliability in the segmentation of brain tumor MRI images.

In a multi-institutional setting, the performance of CNNs in tumor segmentation for glioblastoma patients was strongly influenced by the selection of data used for training.[49] The T1-weighted pre-contrast, T1-weighted post-contrast, and FLAIR images of 44 patients from TCIA GBM data set (http://cancergenome.nih.gov/) were manually segmented by determining tumor components as the ground truth. Three CNN models were trained to automatically segment tumors in patients. The first CNN model was constructed and tested with the images of patients from the same institute. The second CNN model was built with images of patients from one institution and tested with images of patients from the other institute. The third CNN model utilized images of patients from both institutions. The 10-fold cross-validation results showed that the model trained using images from the same institution outperform the model trained on the images from different institution, indicating that images from different institutes may have different characteristics, such as experimental conditions and quality controls. Therefore, images used in training a CNN model impact performance of the model on images from different experimental settings. Determination of the reasons and image aspects for this effect is not clear and deserves further investigation.

Ensemble learning takes advantages of different models to cancel noises in individual models so that prediction accuracy is increased. It has been widely used in diverse domains, including computational toxicology.[12,50–52] Recently, ensemble models were explored for MRI image segmentation. Gupta and Gupta[53] introduced an ensemble architecture that combines 2D and 3D CNNs. Both the 2D and 3D CNN models, as well the ensemble model, were trained and validated using BraTS 2018 data set. The validation results demonstrated that the ensemble model had higher dice scores for segmenting tumor core, whole tumor, and enhancing tumor compared to the individual 2D and 3D CNN models, encouraging utilization of ensemble learning for brain tumor MRI image segmentation. A different ensemble strategy utilizing CNN model was explored for segmenting brain tumor MRI image: a 3D hyper-dense CNN was proposed for volumetric brain tumor segmentation.[54] This network uses 3D fully CNN

for end-to-end volumetric prediction where two 3D CNN configurations (global and local patches) were processed independently and then integrated for final segmentation. The dense connectivity between the two patches provides an opportunity for deep supervision and enhances the flow of gradients during the learning process. This network was hierarchically trained across a few independent paths that were prepared for distinct scale patches and combines local and global feature maps for multi-scale contextual information. Moreover, the bottleneck with a compression model was applied to decrease the quantity of feature maps within every dense block, resulting in a reduction of learned parameters and improving computational efficiency. This model was trained and assessed using the 210 patients' MRI scans in the training data of the BraTS 2018 challenge. The dice scores were the highest for segmenting enhancing tumor and tumor core and segmentation performance on complete tumor ranked second compared to the four CNN models reported in the literature,[46,55–57] again demonstrating that ensemble different learning models improve performance of image segmentation.

Shaikh *et al*.[58] proposed a Tiramisu architecture with 100 layers, developed by combining a post-processing using a dense conditional random field and a densely connected fully CNN, for segmenting brain tumors. This network is composed of the down-sampling path with transition down layers, blocks with densely connected layers, and the up-sampling path with transition up layers. Testing of this network on the BraTS 2017 test set resulted in dice scores of 0.830, 0.650, and 0.650 for the whole tumor, tumor core, and enhanced tumors, respectively, suggesting that this architecture is suitable for brain tumor MRI image segmentation.

An automatic approach for segmenting lesions of brain multi-modal MRI images with 11-layer deep, multi-scale, 3D CNN was proposed.[55] This study utilized a dense training scheme that tackles the calculation challenge in 3D medical scan processing, as well as the issue of imbalanced training samples across different segmentation classes, which has a direct impact on segmentation accuracy. Moreover, a deeper, thus more discriminative,[59] 3D CNN was analyzed followed by a dual pathway architecture for multi-scale processing that incorporates both larger and local contextual data. In additional, a 3D fully connected conditional random field, a 3D extension of the conditional random field model,[60] was applied to process the soft segmentation from the network that effectively removes FPs. Evaluation of this network architecture using the BraTS 2015 test set had dice scores of 0.667, 0.849, and 0.634 for tumor core, whole tumor, and enhanced tumor, respectively, which are better than the compared methods, demonstrating this 3D CNN architecture with parallel convolutional pathways is computationally efficient and suitable for automatic MRI image segmentation.

A computationally efficient CNN architecture to segment brain tumor images was explored[6] to simultaneously utilize both global and local contextual features. Unlike traditional CNN, this network used a fully connected layer convolutionally implemented in the output layer that reduces computation time significantly. Moreover, a two-phase training approach was employed to reduce the impact of the imbalance tumor data, and a cascade architecture was utilized where the output from the primary CNN provides additional information for the succeeding CNN. During the initial training phase, the patches data set is constructed in such a manner that it ensures an equal probability for all labels, effectively addressing the class imbalance. In the subsequent training phase, the output layer is retrained using the true labels distribution to accommodate the imbalanced nature of the data. Testing of the cascade architecture on the BraTS 2013 test set showed dice scores of 0.88, 0.79 for the core tumor, and 0.73 for the whole tumor, tumor core, and enhancing tumor, respectively. The results demonstrate that this architecture performed better than state-of-the-art methods in segmentation accuracy, and also in computational efficiency (30 times faster).

Wang *et al*.[61] developed three fully CNN models to segment brain tumors into three hierarchical subregions (tumor core, whole tumor, and enhanced tumor). The three networks for segmenting tumor core, whole tumor, and enhancing tumor were sequentially connected. During the training stage the ground truth of the tumor core and whole tumor regions were utilized in the second and third stages, respectively, whereas in the testing phase, the tumor core and whole tumor regions obtained from the first and second stages were used in the second and third stages, respectively. Despite the longer training and testing times and the non-end-to-end structure, this cascaded framework has several advantages, including simpler network architectures for each task, reducing over-fitting, being straightforward to train, decreasing FPs, and conforming to the anatomical structure of the brain tumor by employing binary crisp masks.[62] The model was assessed using the BraTS 2017 validation set, which resulted in average dice scores of 0.838, 0.905, and 0.786 for tumor core, whole tumor, and enhanced tumor, respectively. Despite the core tumor region being inside the whole tumor and the enhanced tumor being inside the core tumor region, most of the models did not take this known information into account during modeling. However, the fully CNN models[61] incorporated this information.

Guan *et al*.[63] developed the model AGSE-VNet for segmenting 3D MRI images and included the squeeze and excite (SE) module[64] in the encoder and the attention guide (AG) filter[65] in the decoder in the VNet.[66] The encoder enhances useful information while suppressing useless information. On the other hand, the attention block removes irrelevant background and noise. The guide-image filtering directs image features and structural information, such as edge information. Furthermore, to deal with the issue of imbalance between foreground and background voxels, the categorical dice loss function was employed. Evaluation of AGSE-VNet on the BraTS 2020 validation set showed dice scores of 0.69, 0.85, and 0.68 for tumor core, whole tumor, and enhanced tumor, respectively. However, given the low dice scores for the enhanced tumors and tumor core, there may be room for further improvement.

Zhou *et al*.[67] introduced another modified version of the V-Net model known as the scSE-NL V-Net. This model incorporates two key components: a Spatial and Channel Squeeze-and-Excitation Network (scSE-Net) and a non-local block, which are integrated into the 3D V-Net model. The inclusion of the scSE-Net is intended to enhance the capabilities of

CNN-based image recognition, while the non-local block serves to mitigate inherent image noise interference and compensate for the limited spatial dependence caused by convolution. The scSE-NL V-Net performance was assessed on the BraTS 2020 data set, resulting in Dice scores of 0.82, 0.76, and 0.65 for the entire tumor, tumor core, and enhanced tumor, respectively, on the validation set.

An encoder-decoder based CNN architecture was employed by Myronenko[68] for brain tumor segmentation on 3D MRI images. This CNN architecture has an asymmetrically large encoder and small decoder, incorporating an auto-encoder branch for regularization and utilizing a variational auto-encoder strategy to improve feature clustering, especially when training data is scarce. The ensemble comprising 10 models, all trained from scratch, achieved dice scores of 0.884, 0.815, and 0.766 for the whole tumor, tumor core, and enhanced tumor, respectively, in the evaluation using the BraTS 2018 test set. In addition, the ensemble of one-pass multi-task network and model cascade net, along with their variants,[69] and a deepSCAN architecture[70] showed comparable dice scores when testing on the BraTS 2018 test set. Another modified version of the deepSCAN model,[71] which uses instance normalization to replace batch normalization and incorporates a mechanism with lightweight local attention, achieved dice scores of 0.890, 0.830, and 0.810 for the whole humor, tumor core, and enhanced tumor, respectively, in the evaluation using the BraTS 2019 testing set. Zhao *et al*.[72] modified the self-ensemble U-Net model through various data processing, model designing, and optimizing methods, achieving similar dice scores of 0.883, 0.810, and 0.861 for the whole tumor, enhanced tumor, and tumor core, respectively. These studies demonstrate that the ensemble approach is promising in improving brain tumor MRI image segmentation. A summary of the performance evaluation is shown in Table 3.

U-Net. Ronneberger *et al*.[73] introduced the U-Net model which is a modified and extended version of a fully CNN[74] architecture. It is primarily designed for biomedical image segmentation and can be trained with very few training images. This architecture comprises a contracting path (encoder), an expansive path (decoder), and skip connections. The contracting path consists of a series of convolutions followed by down-sampling with a pooling layer. On the other hand, the expansive path and the contracting path are similar. However, the pooling operations are replaced by up-convolution (up-sampling) operations. Moreover, skip connections combine each up-sample with the relevant cropped feature map in the encoding path. Figure 3 depicts the complete U-Net architecture. The left side represents the contracting path and the right side is the expansive path. The contracting path captures the context information, whereas the expansive path restores the spatial information for pixel-wise segmentation. The skip connections help to retain the spatial information lost during the down-sampling operation. In contrast to the unpadded convolutions used by Ronneberger *et al*.,[73] Dong *et al*.[75] utilized zero-padding for all convolutional layers in both the encoder and decoder to maintain consistent output dimensions in the corresponding layers. Furthermore, they employed a soft loss function based on dice[66] to address the class imbalance issue. Yang and Song[76] constructed a U-Net model using sample preprocessing, optimization algorithm, and the cross-entropy loss function for segmenting brain tumor MRI images. This model was evaluated using the BraTS 2015 challenge training data set, resulting in superior dice scores in both complete and enhanced tumor regions in comparison to the U-Net models reported by Dong *et al*.[75]

Rehman *et al*.[77] introduced BU-Net, a variant of U-Net, that incorporates wide context and residual extended skip modules in the U-Net architecture. The wide context block was used to transition to the decoder from the encoder and the deconvolution layer output was linked with the output yielded from the residual extended skip block of the corresponding encoder block in the skip connection. While the inclusion of these modules facilitates global feature aggregation and contextual information acquisition, the use of 2D convolution in BU-Net results in the loss of context information and local details of different image slices. To handle class imbalance, a loss function that combines dice loss coefficient and weight cross-entropy was used. This loss function leverages the strengths of both loss functions where weight cross-entropy addresses class imbalance by assigning different weights to classes and the dice loss coefficient emphasizes the spatial overlap of true and predicted regions for each class. This U-Net architecture was evaluated on the BraTS 2017 and BraTS 2018 test data sets. This architecture outperformed some state-of-the-art methods, including baseline U-Net,[75] ResU-Net,[78] Seg-Net,[79] PSPNet,[80] NovelNet,[80] 3DU-Net,[81] Ensemble Net,[82] S3DU-Net,[83] TTA,[84] and MCC[85] with similar cost functions, optimizers, and cofactors. However, it requires further investigation to determine if the compared models can perform better in different algorithmic settings.

Ghosh *et al*.[86] developed an improved U-Net architecture that incorporates pre-trained VGG-16 layers in transitioning to the decoder from the encoder. In addition, dense-convolutional blocks were used for down-sampling in this model, which improves feature re-usability. The use of batch normalization layers within dense blocks also enhanced the model's stability and performance. This U-Net architecture was evaluated using the low-grade glioma data set from TCIA.[87] This model exclusively focused on segmenting tumor cells and achieved a dice coefficient of 0.93 in a fivefold cross-validation, which is much higher than the 0.68 dice coefficient of the basic U-Net, suggesting the incorporated layers in this improved U-Net enhance segmentation accuracy.

Wibowo *et al*.[88] presented a 2D U-Net model that employs HeNormal initialization to avoid the issues of gradient explosion and vanishing. In addition, batch normalization was applied in the first pooling layer to normalize the output and prevent loss overfitting. The gradient computation dropout was used to connect the encoder and decoder. This model was assessed using the BraTS 2018 and BraTS 2020 data sets and resulted in dice scores of 0.90 and 0.92 for classifying whole tumor regions for the BraTS 2018 and BraTS 2020 data sets, respectively.

Table 3. Performance of CNN models based on BraTS data sets.

Data set	Dice score								
	Cross-validation			Validation set			Test set		
	WT	TC	ET	WT	TC	ET	WT	TC	ET
BRATS 2013[47]	–	–	–	0.84	0.72	0.62	0.88	0.83	0.77
BRATS 2013[6]				0.84	0.71	0.57	0.88	0.79	0.73
BRATS 2013[56]	–	–	–	0.86	0.73	0.62	0.87	0.83	0.76
BRATS 2015[47]	–	–	–	–	–	–	0.78	0.65	0.75
BRATS 2015[55]	0.90	0.75	0.73	–	–	–	0.85	0.67	0.63
BRATS 2017[57]	0.72	0.83	0.81	–	–	–	–	–	–
BRATS 2017[58]	–	–	–	0.87	0.68	0.65	0.83	0.65	0.65
BRATS 2017[61]	–	–	–	0.91	0.84	0.79	0.87	0.77	0.78
BRATS 2018[54]	0.87	0.84	0.81	–	–	–	–	–	–
BRATS 2018[68]	–	–	–	0.91	0.87	0.82	0.88	0.82	0.77
BRATS 2018[69]	–	–	–	0.91	0.87	0.81	0.88	0.80	0.78
BRATS 2018[70]	–	–	–	0.90	0.85	0.80	0.89	0.80	0.73
BRATS 2018[53]	0.90	0.87	0.80	–	–	–	–	–	–
BRATS 2019[71]	–	–	–	0.91	0.83	0.77	0.89	0.83	0.81
BRATS 2019[72]	–	–	–	0.91	0.84	0.75	0.88	0.86	0.81
BRATS 2020[63]	0.85	0.77	0.70	0.85	0.69	0.68	–	–	–
BRATS 2020[67]	–	–	–	0.82	0.76	0.65	–	–	–

CNN: convolutional neural network; BRATS: brain tumor segmentation challenge; WT: whole tumor; TC: tumor core; ET: enhanced tumor.

ResU-Net,[78] another variant of U-Net, replaces the plain blocks in both the decoder and encoder of the U-Net model with residual blocks.[89,90] Residual blocks include a shortcut mechanism to prevent the gradients from vanishing and lead to faster convergence by integrating the global features with rough local. In addition, a residual unit was utilized as a bridge to connect the encoder and decoder. To address the imbalance issue in brain tumor MRI images, the authors implemented a loss function that combines weighted cross-entropy[91] with generalized dice loss.[92] This U-Net architecture was assessed using the BraTS 2018 data set, resulting in average dice scores 0f 0.805, 0.868, and 0.783 for tumor core, whole tumor, and enhancing tumor, respectively, making this U-Net a top performed model in the BraTS 2018 challenge. This demonstrates that this U-Net model may be used for brain tumor MRI image segmentation in clinical practices.

Zhang *et al*.[93] developed an AResU-Net model that adds the attention and squeeze excitation block on the skip connections in the ResU-Net model to adaptively improve local reactions of down-sampling features that can be applied to the feature recovery in subsequent up-sampling process. This can decrease the semantic gap between the up-sampling and down-sampling processes. Incorporating the attention and squeeze excitation block on the skip connections in the ResU-Net[78] model yielded improved model performance on both the BraTS 2018 and BraTS 2017 data sets. The dice scores of 0.780, 0.881, and 0.719 for tumor core, whole tumor, and enhancing tumor, respectively, were obtained in testing 20% of the BraTS 2017 training set with the model trained on 80% of the training set. Similar dice scores of 0.810, 0.876, and 0.773 for tumor core, whole tumor, and enhancing tumor, respectively, were obtained when testing the BraTS 2018 validation set with the U-Net model trained on the BraTS 2018 training set, which outperformed most of the compared models, especially for enhancing tumor segmentation. However, this U-Net architecture underperformed S3DU-Net.[83] which achieved better dice scores of 0.831 and 0.894 for tumor core and whole tumor segmentations, respectively.

Since 2D convolutions are unable to make use of the spatial information present in volumetric image data, a 3D extension of the 2D U-Net model was proposed[81] to replace all 2D operations in the 2D U-Net[73] model with their 3D counterparts. The 3D U-Net model with slight modifications performed best in the BraTS 2018 and BraTS 2017 challenges with dice scores of 0.775, 0.858, and 0.647 on the BraTS 2017 test set,[94] and slightly better dice scores of 0.806, 0.878, and 0.779 on the BraTS 2018 test set[95] for tumor core, whole tumor, and enhancing tumor, respectively.

A similar 3D U-Net model was implemented by Mehta and Arbel[96] with some modifications, such as replacing the max pooling in the encoder with average pooling to get better gradient flow between consecutive layers, applying instance normalization[97] followed by a dropout[98] with 0.05 probability to get memory advantage in both encoder and decoder. Furthermore, the model employs a loss function weighted by categorical cross-entropy and utilizes a curriculum class weighting method to tackle the class imbalance problem. The performance of this U-Net model was assessed on the BraTS 2018 data set by fivefold cross-validation, which resulted in dice scores of 0.793, 0.888, and 0.690 for tumor core, whole tumor, and enhanced tumor, respectively. The model also performed well on the BraTS 2018 validation set with dice scores of 0.825, 0.909, and 0.788 for tumor core, whole tumor, and enhanced tumor, respectively. It is noteworthy that the model exhibited notably superior performance on the validation set, particularly for enhanced tumor prediction, which may warrant further investigation.

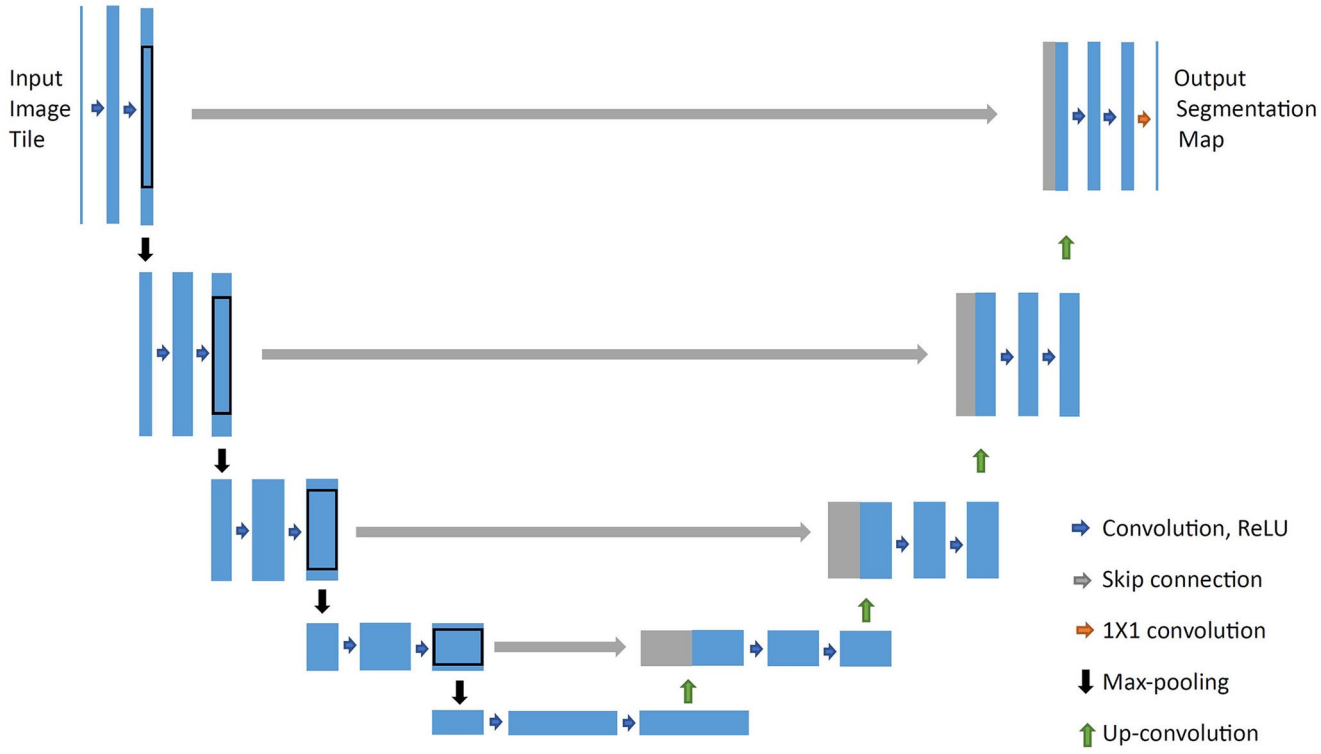

Figure 3. Illustration of general U-Net Architecture. Each blue box represents a multi-channel feature map. The number of channels can be different for the input image tile. The white boxes represent copied feature maps. The arrows denote the different operations as shown in the legend at right bottom. Max-pooling and up-convolution usually take 2×2.

Jiang *et al*.[99] introduced a two-stage cascaded U-Net model where the MRI modalities process an initial rough segmentation and provide a more accurate segmentation map in the second stage with additional network parameters. In addition, a post-processing step was conducted, wherein enhancing tumors were replaced with necrosis if the volume of the enhancing tumor prediction falls below a specific threshold. This threshold is chosen independently for each experiment. To reduce variability, an ensemble of 12 models was built from scratch using the complete training data set. The ensemble performed well on both the BraTS 2019 validation and test data sets. The dice scores of ensembles on the BraTS 2019 test set were 0.837 for tumor core, 0.888 for whole tumor, and 0.833 for enhanced tumor, ranking first in the challenge. However, the ensemble of 12 models did not exhibit a significant performance improvement compared to the best individual model in the validation set. It is worth noting that the performance of an ensemble model depends on the ensemble method used (e.g. majority votes, weighted sum, boosting).

Instead of combining all four modalities at the network input, in the modality-pairing network[100] the modalities were divided into two groups (T1 and post-contrast T1-weighted in one group, and FLAIR and T2-weighted in the other group) and simultaneously processed using parallel branches. Notably, the same 3D U-Net architecture was shared by both branches. This method was tested on the BraTS 2020 data set. The top three single Vanilla U-Net models and three single modality-pairing models, chosen based on their performance in the fivefold cross-validation on the validation data set, were included in the ensemble model. The resulting dice scores on the BraTS 2020 validation set (test set) using this ensembled model were 0.856 (0.842) for tumor core, 0.908 (0.891) for whole tumor, and 0.787 (0.816) for enhanced tumor. The ensemble model ranked second in the BraTS 2020 challenge, demonstrating that ensembles of different models is an attractive strategy for brain tumor MRI image segmentation.

Scale attention network (SA-Net) is derived from the encoding-decoding architecture with a larger encoding pathway, a smaller decoding pathway, and scale attention blocks. Moreover, unlike U-Net, this model has full scale skip connections. This network was challenged on the BraTS 2020 data set (369 cases) and outperformed the Vanilla U-Net model. High dice scores of 0.8773, 0.9151, and 0.8125 were achieved for tumor core, whole tumor, and enhanced tumors, respectively, in fivefold cross-validation with the training set.[101] Subsequently, in the fivefold cross-validation on the BraTS 2021 data set (1251 cases), the SA-Net obtained dice scores of 0.9211, 0.9372, and 0.8843 for tumor core, whole tumor, and enhanced tumors, respectively, indicating that segmentation performance can be significantly enhanced with larger data sets.[102]

3D convolution is computationally expensive and requires high memory. To address these issues, Chen *et al*.[83] developed a separable 3D U-Net (S3D-Unet) architecture by replacing 3D convolutions with spatiotemporal-separable 3D (S3D) convolutions, which was proposed by Xie *et al*.,[103] in both encoder and decoder. The S3D convolution replaces each 3D convolution with a combination of two connected

Table 4. Comparison among different variant of the U-Net model.

Variant name [Reference]	Loss function	Remark
U-Net[73]	Cross-entropy	Consists of a contracting path (encoder), an expansive path (decoder) and skip connections, and can train the model with a limited training data set
BU-Net[77]	Sum of weight cross-entropy and Dice loss coefficient	Residual extended skip (RES) and wide context (WC) are embedded in the U-Net model
ResU-Net[78]	Sum of weight cross-entropy and generalized Dice loss	Plain blocks in both the encoder and decoder of the U-Net model are replaced with residual blocks. A residual unit is also utilized as a bridge to connect the encoder and decoder
AresU-Net[93]	Sum of weight cross-entropy and generalized Dice loss	Embeds the attention and squeeze excitation (ASE) block on the skip connections in the ResU-Net model
3D U-Net[81]	Weight cross-entropy	Replaces all 2D operations in the 2D U-Net[65] model with their 3D counterparts
S3D-Unet[83]	Dice loss	Replaces each 3D convolution in 3D U-Net with spatiotemporal-separable 3D counterparts
MBANet[104]	Generalized Dice loss	The encoder and decoder are constructed combining the basic unit (BU) module and the multi-branch 3D SA module, and the multi-branch 3D SA module is applied as the attention of the skip connection
nnU-Net[109]	Sum of cross-entropy and Dice loss	Develops three separate configurations (2D U-Net, 3D U-Net, or 3D U-Net cascade) and automatically picks the best model (or combination of two) based on the average foreground Dice coefficient

RES: residual extended skip; WC: wide context; ASE: attention and squeeze excitation; BU: basic unit.

convolutional layers: a 1D convolution to extract temporal features and a 2D convolution to extract spatial features. This architecture was evaluated using the BraTS 2018 data sets. The results of fivefold cross-validation on the BraTS 2018 training set yielded mean dice scores of 0.844, 0.888, and 0.740 for tumor core, whole tumor, and enhancing tumor, respectively, which are comparable to corresponding dice scores 0.868, 0.899, and 0.684 of the 3D U-Net without the S3D block.

Cao *et al*.[104] proposed a 3D CNN with 3D multi-branch attention (MBANet) for segmenting brain tumor MRI images using the 3D shuffle attention module. The encoder and decoder were constructed using both the basic unit module and the multi-branch 3D shuffle attention module, which allows the network to improve its feature fusion capabilities without significantly increasing the computational requirements. In addition, the multi-branch 3D shuffle attention module was applied as the attention of the skip connection, resulting in a more rational organization of both channel attention and spatial attention mechanisms. MBANet was assessed using the BraTS 2019 and BraTS 2018 data sets. The fivefold cross-validation of MBANet resulted in dice scores of 0.860, 0.900, and 0.775 on the BraTS 2018 training set and 0.851, 0.899, and 0.789 on the BraTS 2019 training set for tumor core, whole tumor, and enhancing tumor, respectively. These results demonstrate superior performance of MBANet compared to other models.[83,105–108]

Recently, nnU-Net, introduced by Isensee *et al*.,[109] has gained popularity as a leading method for segmenting biomedical images because of its automatic adaptability to new data sets and improved performance. The fully open-source codes and models have contributed to its widespread adoption. Since it is difficult to estimate which U-Net configuration performs the best on what data set, nnU-Net develops three separate configurations (3D U-Net, 2D U-Net, or 3D U-Net cascade) and automatically picks the best model according to the average foreground dice score calculated from cross-validation on the training data. Isensee *et al*.[110] and Luu and Park[111] applied the nnU-Net model with some modifications to the BraTS 2021 BraTS 2020 challenge data sets, respectively. However, both Isensee *et al*.[110] and Luu and Park[111] selected the final models for the test data sets based on their performance on the validation sets, rather than based on cross-validation results. On the BraTS 2020 test set, dice scores of 0.851, 0.890, and 0.820 were obtained for tumor core, whole tumor, and enhanced tumor, respectively, and the BraTS 2021 test set yielded corresponding dice scores of 0.888, 0.931, and 0.884. The notable increase in the dice scores on the BraTS 2021 data set compared to the BraTS 2020 data set may be connected with the increase in training data size, 369 cases to 1251 cases.

Table 4 presents a concise comparison of several variants of the U-Net model and highlights the growing trend of utilizing combined loss functions compared to single loss functions. Because different loss functions can capture different aspects of the learning problem, combining them can help guide the model's learning process more effectively. Table 5 displays a performance comparison among several variants of the U-Net model on the BraTS challenge data sets. Generally, for the same model the dice score positively correlates with tumor size (enhancing tumor $<$ tumor core $<$ whole tumor), possibly due to the significant impact of misclassifications or segmentation errors in smaller regions. Furthermore, the model performance on the BraTS 2021 data set showed a significant improvement compared to other data sets. One possible reason for this improvement is the increase in training data size.

Hybrid methods

Hybrid methods in image segmentation refer to the combination of two or more algorithms or techniques to enhance robustness and precision of the segmentation results. It is worth noting that different from ensemble methods which

Table 5. Performance of U-Net models based on BraTS data sets.

Model name	Data set	Dice score								
		Cross-validation			Validation set			Test set		
		WT	TC	ET	WT	TC	ET	WT	TC	ET
U-Net[75]	BraTS 2015	0.860	0.860	0.650	–	–	–	–	–	–
U-Net[76]	BraTS 2015 (HGG)	0.900	0.820	0.870	–	–	–	–	–	–
3D U-Net[94]	BraTS 2017	0.895	0.828	0.707	0.896	0.797	0.732	0.858	0.775	0.647
BU-Net[77]	BraTS 2017	0.892	0.783	0.736	–	–	–	–	–	–
AResU-Net[93]	BraTS 2017	0.881	0.780	0.719	–	–	–	–	–	–
ResU-Net[78]	BraTS 2018	0.888	0.793	0.690	0.909	0.825	0.788	0.871	0.771	0.706
3D U-Net[96]	BraTS 2018	0.888	0.844	0.740	0.894	0.831	0.749	0.839	0.783	0.689
S3DU-Net[83]	BraTS 2018	0.918	0.857	0.786	0.913	0.863	0.809	0.878	0.806	0.779
No new-Net[95]	BraTS 2018	–	–	–	0.901	0.837	0.788	–	–	–
BU-Net[77]	BraTS 2018	–	–	–	0.876	0.810	0.773	–	–	–
AresU-Net[93]	BraTS 2018	0.900	0.860	0.775	0.898	0.855	0.802	–	–	–
MBANet[104]	BraTS 2018	–	–	–	0.909	0.865	0.802	0.888	0.837	0.833
Two-stage cascaded U-net[99]	BraTS 2019	0.924	0.898	0.863	0.908	0.856	0.787	0.891	0842	0.816
MBANet[104]	BraTS 2019	0.915	0.877	0.813	0.911	0.853	0.793	0.883	0.843	0.818
nnU-Net[110]	BraTS 2020	0.937	0.921	0.884	0.927	0.866	0.848	0.928	0.885	0.875
3D U-Net[100]	BraTS 2020	0.938	0.924	0.882	0.928	0.878	0.845	0.930	0.890	0.880
SA-Net[101]	BraTS 2020	0.860	0.860	0.650	–	–	–	–	–	–
SA-Net[102]	BraTS 2021	0.895	0.828	0.707	0.896	0.797	0.732	0.858	0.775	0.647
nnU-Net[111]	BraTS 2021	0.892	0.783	0.736	–	–	–	–	–	–

BRATS: Brain Tumor Segmentation Challenge; WT: whole tumor; TC: tumor core; ET: enhanced tumor.

combine predictions from different algorithms to make a consensus prediction using a voting strategy, algorithms in a hybrid method synergistically work to predict a single outcome, with no voting element involved. These techniques improve the segmentation performance by utilizing the advantages of various algorithms and offsetting their limitations.

Aboelenein *et al*.[112] developed a novel architecture, hybrid two-track U-Net (HTTU-Net), for brain tumor segmentation. HTTU-Net showed superior performance in handling class imbalance data compared to the original U-Net architecture and can alleviate overfitting issue. This architecture is composed of two tracks with varying numbers of layers and kernel sizes. The first track concentrates on the form and size of tumor. The second track extracts the contextual information. Batch normalization was applied after each convolution block followed by a Leaky Relu activation function to alleviate the variance and mean problems and to stabilize the layers. The results of both tracks were then combined, and the final segmentation output was generated from this concatenation. A hybrid loss function integrating the generalized dice loss and focal loss functions was employed to mitigate the class imbalance. Focal loss is a modified version of the conventional cross-entropy loss function and assigns more focus to the minority classes and misclassified samples. In contrast, the dice loss coefficient focuses on the spatial overlap of true and predicted regions for each class. The BraTS 2018 challenge data sets were utilized to evaluate this model's performance, resulting in an increase of 0.014, 0.013, and 0.055 in the dice scores for tumor core, whole tumor, and enhancing tumor, respectively, when compared to the original U-Net.

The baseline U-Net model has several shortcomings.[113,114] First, brain tumors are irregular in structure and exhibit size variation, making it challenging to train a model to accurately generalize tumor structure. The traditional U-Net model can detect the correct region of interest, but it tends to over-segment the area. Second, in the U-Net model, skip connections combine the high-level features of decoder and the low-level features from encoder. This merging can create a semantic gap between the two types of features, which can affect the baseline U-Net model's performance. Third, small brain tumors are hard to locate and segment. The baseline U-Net model struggles to differentiate between small tumor regions and many background pixels. Fourth, the baseline U-Net model produces numerous feature maps that look alike, but only a small fraction of them are useful in learning the actual task. To overcome these shortcomings a hybrid U-Net model consisting of several resolution blocks, dual attention blocks, residual blocks, and a deep supervision block was proposed.[114] The multiple resolution blocks extract features and analyze tumors with different scales; residual blocks extract features to decrease the semantic gap between the high-level features of skip connections and the low-level features of the decoder; dual attention mechanisms emphasize tumor representations and demote over-segmentation; and deep supervision blocks use features of decoder layers to generate the target segmentation. In addition to the dice score, Hausdorff distance, which represents the largest error of segmentation, was used to evaluate model performance.[115] An outlier refers to a data point that significantly deviates from the norm or the expected pattern within an MRI image. To mitigate the impact of outliers, the Hausdorff distance was calculated using only the top 95% of distances from

the complete set of minimum distances. The validation and training data sets of BraTS 2020 challenge were used to build and evaluate this hybrid model. The results showed that this hybrid U-Net model outperformed the baseline U-Net in terms of both Hausdorff score and dice score, indicating that the hybrid model can produce more accurate segmentation results but may over-segment the tumor area.

Three hybrid CNNs (U-SegNet, Seg-Unet, and Res-SegNet) were explored for the segmentation of brain tumor MRI images using a pairwise combination of three popular CNNs (SegNet, U-Net, and ResNet18).[77] The SegNet architecture has two types: SegNet3 containing three convolution blocks and SegNet5 containing five convolution blocks.[79] While U-SegNet is the fusion of SegNet3 and U-Net,[116] Seg-Unet is the combination of U-Net and SegNet5. On the other hand, Res-SegNet is a hybrid of SegNet5 and ResNet18. During down-sampling, small brain tumors can be lost, which can result in inaccurate segmentation. Inspired by Res-Net18 and U-Net, these hybrid models are able to solve such problems by including a skip connection in the SegNet. The performance of these models was evaluated using the BraTS data sets. The mean Jaccard similarity coefficients of the U-Net, U-SegNet, Res-SegNet, SegNet3, SegNet5, and Seg-Unet models were 0.592, 0.648, 0.689, 0.536, 0.602, and 0.734, respectively, which indicates that the hybrid models outperformed SegNet3, SegNet5, and U-Net models. Notably, Seg-Unet demonstrated the highest performance among all the models, producing well-segmented result with accurate boundary alignment for each class.

The hybrid pyramid U-Net (HPU-Net)[117] consists of three modules, a down-sampling path, a symmetrical up-sampling path, and an additional segmentation path using the image pyramid. The down-sampling path includes a batch normalization[118] layer inside each block. The block contains two 3×3 kernel convolutional layers, two batch normalization layers, and a layer with 2×2 strides for max pooling. The task of the batch normalization layers is to avoid gradient vanishing during back propagation and to accelerate the model convergence. The convolutional layers prevent the disappearance of small lesion areas during down-sampling. While the down-sampling path extracts global contextual and high-level features of a tumor, the up-sampling path reconstructs object details. The auxiliary path extracts multi-scale information and combines location and semantic information in the up-sampling path to help the model segment objects with various scales. The high-level features contain semantic information, whereas the low-level features contain location information. The BraTS 2015 and BraTS 2017 challenge data sets were used to train and evaluate this model and the results showed that this hybrid model outperformed the brain tumor MRI image segmentation methods at the most recent stage.

Kamnitsas *et al*.[119] proposed EMMA (ensemble of multiple models and architectures) that integrates widely varying CNNs. Specifically, EMMA incorporated three 3D fully convolutional networks (FCNs), two deepMedic models, and two 3D versions of the U-Net models. All models were trained independently. However, during the testing phase, each model was used to segment an unobserved image separately and generate corresponding class-confidence maps. These models were then ensembled into EMMA that takes the average of the probabilities from individual models. Since EMMA creates a robust system that remains insensitive to independent failures of CNN components, this approach yielded impressive dice scores on the test and validation sets of the BraTS 2017 challenge.

Jia *et al*.[120] proposed another hybrid model, hybrid high-resolution and non-local feature network (H^{2}NF-Net), which concurrently employed both single and cascaded HNF-Nets. This model employs an ensemble of 27 models, including five single models built in fivefold cross-validation, five cascaded models constructed in fivefold cross-validation, seven single models developed using the entire training set, and 10 cascaded models constructed from the entire training set. On the validation set of BraTS 2020, it achieved dice scores of 0.855, 0.913, and 0.788 for tumor core, whole tumor, and enhanced tumor, respectively. However, an ensemble of seven single models trained with the entire training set exhibited comparable performance with dice scores of 0.849, 0.912, and 0.789 for tumor core, whole tumor, and enhanced tumor, respectively. On the BraTS 2020 test set, the H^{2}NF-Net model achieved dice scores of 0.854, 0.888, and 0.828 for tumor core, whole tumor, and enhanced tumor, respectively.

A hybrid technique that combines both texture-based method and region-based method was proposed for brain tumor segmentation and classification based on MRI images.[121] In this method, a gray-level co-occurrence matrix was utilized as the texture-based method to extract features from MRI images and a fast bounding box algorithm[122] was applied as the region-based method for segmenting tumors. The two least squares SVM classifiers, one combined with the multi-layer perceptron-based kernel function and another combined a kernel of radial basis function, was employed to classify the features generated from the feature extraction stage as tumorous or non-tumorous images. Moreover, the noise of MRI images was removed by median filtering followed by skull detection using boundary detection criteria in the pre-processing step. Using the images in the BraTS challenge data sets, 10-fold cross-validation was used to construct and test the least squares SVM classifiers with the two kernel functions. The results showed that the least squares SVM classifier containing a multi-layer perceptron kernel function reached a very promising accuracy (96.63%) in the 10-fold cross-validation. Furthermore, it demonstrated superior performance compared to various classifiers, including the least squares SVM classifier, neural network with back propagation,[123] neural network with radial basis function,[123] AdaBoost classifier,[124] and SVM models.[125]

The fuzzy c-means algorithm is a popular segmentation method of brain tissues, known for its robustness and effectiveness in identifying similar brain tissues and localization. It involves minimizing an objective function and provides superior results in both convergence rate and segmentation efficiency.[126] On the other hand, Hopfield neural network (HNN) was used to solve optimization problems using Lyapunov energy function, where accuracy depends on the weighting factors applied in the energy function, and stability of the network was achieved when the modified Lyapunov energy function reaches its minimum.[127] The fuzzy HNN is a hybridization of fuzzy c-means and HNN that

Table 6. Performance of hybrid models based on BraTS data sets.

Model name	Data set	Dice score								
		Cross-validation			Validation set			Test set		
		WT	TC	ET	WT	TC	ET	WT	TC	ET
HPU-Net[117]	BRATS 2015	0.91	0.72	0.79	–	–	–	–	–	–
HPU-Net[117]	BRATS 2017	0.92	0.80	0.76	–	–	–	–	–	–
EMMA[119]	BRATS 2017	–	–	–	0.90	0.80	0.74	0.89	0.79	0.73
HTTU-Net[112]	BRATS 2018	0.87	0.81	0.75	–	–	–	–	–	–
H^2NF[120]	BRATS 2020	–	–	–	0.91	0.85	0.79	0.89	0.85	0.83
MultiResUNet [114]	BRATS 2020	0.95	0.93	0.82	0.75	0.62	0.60	–	–	–

BRATS: Brain Tumor Segmentation Challenge; WT: whole tumor; TC: tumor core; ET: enhanced tumor; EMMA: ensemble of multiple models and architectures.

enables efficient parallel implementation of online learning for image segmentation. The objective function of the fuzzy HNN was minimized by a modified Lyapunov energy function based on unsupervised 2D fuzzy HNN. While searching for the optimal weighting factors is laborious and time-consuming, the fuzzy HNN can easily solve this problem.[128] This hybrid method was quantitatively validated using two MRI modalities—T1- and T2-weighted.[87] The mean Jaccard similarity score, dice score, specificity, and sensitivity of the final segmentation were 0.8569, 0.9186, 0.9917, and 0.9480, respectively. Although the fuzzy HNN may encounter difficulties in differentiating between different brain tissues in MRI images that have low tissue contrast, a possible solution was proposed.[129] The GMM on the input MRI images was recommended, as this model can enhance the image's brightness, content, and contrast, ultimately overcoming the difficulties posed by low tissue contrast.

A hybrid approach integrating fuzzy c-means and K-means algorithms was developed to accurately detect brain tumors in the minimal time since K-means is faster and fuzzy c-means is able to detect tumor cells more accurately.[130] Moreover, this hybrid approach overcomes the limitations of the original fuzzy c-means algorithm in segmenting MRI images that contain artifacts, such as outliers and noise. Thresholding and active contour-level set segmentation methods are then used to accurately detect brain tumors. The performance of this model was evaluated using three benchmark data sets: BraTS 2012, Brain Web, and DICOM (Digital Imaging and Communications in Medicine). This integrating method is more computationally demanding than the K-means method, but it is faster than the fuzzy c-means algorithms. Despite this, this integrating method achieved the highest accuracy when testing on all the three data sets. The performance evaluation comparison among different hybrid models is presented in Table 6.

Limitations

Medical image segmentation is a complex task that poses several challenges, such as identifying the intricate and subtle boundaries of organs, limited uniformity and similarity within regions of interest, low contrast and intensity in homogeneity, and image noise. In addition, brain tumor MRI image segmentation involves many steps, including preprocessing, feature extraction, and segmentation. Therefore, the precision of segmentation is intricately linked to the precision of each step. Class imbalance is a major issue to handle brain tumor MRI image segmentation. Only a small sub-region has tumors, and thus the non-tumor tissues play a dominant role in shaping the class distribution. The heterogeneity of brain tumors also makes it difficult to accurately segment the tumor as different tumor regions may necessitate distinct segmentation approaches. To our knowledge, there is no method mentioned in the existing literature that consistently delivers the top performance across all evaluation parameters.

Though many methods based on machine learning and deep learning techniques have been explored for segmentation of brain tumor MRI images, no such methods have been implemented in software tools that are adopted in clinical decision-making. Multiple challenges impeded the translation of the developed machine learning and deep learning models to clinical practice. The first difficulty is the lack of an adequate amount of annotated brain tumor MRI images. Lack of high-quality annotated brain tumor MRI images for training limits segmentation accuracy of the developed methods, hindering their utilization in clinical practice. Most of the developed methods are based on the BraTS data sets that contain four types of images annotated by radiologists. However, brain tumors can vary widely in terms of size, shape, location, and appearance in MRI images. This variability makes the models developed using BraTS data sets difficult to the one-size-fits-all models for brain tumor MRI images obtained in different clinical sites. In clinical practice, there is a need for real-time or near-real-time tumor segmentation, especially during surgeries. Many current segmentation models developed using machine learning and deep learning algorithms may not meet these real-time requirements, which obstruct their application in clinical practice.

Conclusions

The task of segmenting brain tumor MRI images is difficult. However, publicly accessible data sets have created a shared platform for researchers to develop and compare their techniques. This review article presents various machine learning and deep learning approaches that have been used for brain tumor MRI image segmentation. While both techniques have the potential to enhance efficiency and accuracy in brain tumor MRI image segmentation, each has its own

limitations. Machine learning techniques may face computational challenges when dealing with a large number of observations, whereas deep learning techniques require a significant amount of data to train models, otherwise, the predictive performance may suffer.[131] Despite this, deep learning techniques have demonstrated better performance than traditional machine learning techniques in this field. Hybrid methods have shown promising results by combining the strengths of different techniques. However, there are still challenges to be addressed, including the selection of appropriate algorithms, as well as the interpretation and validation of results in a clinical context. Thus, further research is needed to validate the effectiveness of these techniques in the real-world clinical setting.

AUTHORS' CONTRIBUTIONS

MKHK, WG, JL, FD, ZL, HH reviewed the literature. MKHK and HH wrote the first draft. TP revised the manuscript. All authors have reviewed and agreed to the published version of the manuscript.

ACKNOWLEDGEMENTS

This research was supported in part by an appointment to the Research Participation Program at the National Center for Toxicological Research (Md Kamrul Hasan Khan and Zoe Li), administered by the Oak Ridge Institute for Science and Education through an interagency agreement between the US Department of Energy and the US Food and Drug Administration.

DECLARATION OF CONFLICTING INTERESTS

The author(s) declared no potential conflicts of interest with respect to the research, authorship, and/or publication of this article.

FUNDING

The author(s) received no financial support for the research, authorship, and/or publication of this article.

DISCLAIMER

This article reflects the views of the authors and does not necessarily reflect those of the U.S. Food and Drug Administration.

ORCID IDS

Md Kamrul Hasan Khan https://orcid.org/0009-0004-9835-5594
Wenjing Guo https://orcid.org/0000-0002-0814-6982
Jie Liu https://orcid.org/0000-0001-6988-5773
Huixiao Hong https://orcid.org/0000-0001-8087-3968

REFERENCES

1. Bahadure NB, Ray AK, Thethi HP. Image analysis for MRI based brain tumor detection and feature extraction using biologically inspired BWT and SVM. *Int J Biomed Imaging* 2017;**2017**:9749108
2. Işın A, Direkoğlu C, Şah M. Review of MRI-based brain tumor image segmentation using deep learning methods. *Proc Comput Sci* 2016;**102**:317–24
3. Shen S, Sandham W, Granat M, Sterr A. MRI fuzzy segmentation of brain tissue using neighborhood attraction with neural-network optimization. *IEEE T Inf Technol Biomed* 2005;**9**:459–67
4. Bhargava R, Hahn G, Hirsch W, Kim MJ, Mentzel HJ, Olsen OE, Stokland E, Triulzi F, Vazquez E. Contrast-enhanced magnetic resonance imaging in pediatric patients: review and recommendations for current practice. *Magn Reson Insights* 2013;**6**:95–111
5. Gordillo N, Montseny E, Sobrevilla P. State of the art survey on MRI brain tumor segmentation. *Magn Reson Imaging* 2013;**31**:1426–38
6. Havaei M, Davy A, Warde-Farley D, Biard A, Courville A, Bengio Y, Pal C, Jodoin P-M, Larochelle H. Brain tumor segmentation with deep neural networks. *Med Image Anal* 2017;**35**:18–31
7. Sharif MI, Li JP, Khan MA, Saleem MA. Active deep neural network features selection for segmentation and recognition of brain tumors using MRI images. *Patter Recogn Lett* 2020;**129**:181–9
8. Bauer S, Wiest R, Nolte L-P, Reyes M. A survey of MRI-based medical image analysis for brain tumor studies. *Phys Med Biol* 2013;**58**:R97–129
9. Baid U, Ghodasara S, Mohan S, Bilello M, Calabrese E, Colak E, Farahani K, Kalpathy-Cramer J, Kitamura FC, Pati S, Prevedello LM, Rudie JD, Sako C, Shinohara RT, Bergquist T, Chai R, Eddy J, Elliott J, Reade W, Schaffter T, Yu T, Zheng J, Moawad AW, Coelho LO, McDonnell O, Miller E, Moron FE, Oswood MC, Shih RY, Siakallis L, Bronstein Y, Mason JR, Miller AF, Choudhary G, Agarwal A, Besada CH, Derakhshan JJ, Diogo MC, Do-Dai DD, Farage L, Go JL, Hadi M, Hill VB, Iv M, Joyner D, Lincoln C, Lotan E, Miyakoshi A, Sanchez-Montano M, Nath J, Nguyen XV, Nicolas-Jilwan M, Jimenez JO, Ozturk K, Petrovic BD, Shah C, Shah LM, Sharma M, Simsek O, Singh AK, Soman S, Statsevych V, Weinberg BD, Young RJ, Ikuta I, Agarwal AK, Cambron SC, Silbergleit R, Dusoi A, Postma AA, Letourneau-Guillon L, Perez-Carrillo GJG, Saha A, Soni N, Zaharchuk G, Zohrabian VM, Chen Y, Cekic MM, Rahman A, Small JE, Sethi V, Davatzikos C, Mongan J, Hess C, Cha S, Villanueva-Meyer J, Freymann JB, Kirby JS, Wiestler B, Crivellaro P, Colen RR, Kotrotsou A, Marcus D, Milchenko M, Nazeri A, Fathallah-Shaykh H, Wiest R, Jakab A, Weber M-A, Mahajan A, Menze B, Flanders AE, Bakas S. The RSNA-ASNR-MICCAI BraTS 2021 benchmark on brain tumor segmentation and radiogenomic classification. *Arxiv Preprint* 2021, https://arxiv.org/abs/2107.02314
10. Luo H, Ye H, Ng HW, Shi L, Tong W, Mendrick DL, Hong H. Machine learning methods for predicting HLA-peptide binding activity. *Bioinform Biol Insights* 2015;**9**:21–9
11. Ye H, Tang K, Feuers R, Hong H. Drug repositioning through network pharmacology. *Curr Topics Med Chem* 2016;**16**:3646–56
12. Hong H, Tong W, Xie Q, Fang H, Perkins R. An in silico ensemble method for lead discovery: decision forest. *SAR QSAR Environ Res* 2005;**16**:339–47
13. Huang Y, Li X, Xu S, Zheng H, Zhang L, Chen J, Hong H, Kusko R, Li R. Quantitative structure–activity relationship models for predicting inflammatory potential of metal oxide nanoparticles. *Environ Health Perspect* 2020;**128**:67010
14. Wang Z, Chen J, Hong H. Developing QSAR models with defined applicability domains on PPARγ binding affinity using large data sets and machine learning algorithms. *Environ Sc Technol* 2021; **155**:6857–66
15. Liu J, Guo W, Dong F, Aungst J, Fitzpatrick S, Patterson TA, Hong H. Machine learning models for rat multigeneration reproductive toxicity prediction. *Front Pharmacol* 2022;**13**:1018226
16. Zhang C, Shen X, Cheng H, Qian Q. Brain tumor segmentation based on hybrid clustering and morphological operations. *Int J Biomed Imaging* 2019;**2019**:7305832
17. Kaya IE, Pehlivanlı AÇ, Sekizkardeş EG, Ibrikci T. PCA based clustering for brain tumor segmentation of T1w MRI images. *Comput Method Program Biomed* 2017;**140**:19–28
18. Şişik F, Sert E. Brain tumor segmentation approach based on the extreme learning machine and significantly fast and robust fuzzy C-means clustering algorithms running on Raspberry Pi hardware. *Med Hypotheses* 2020;**136**:109507
19. Ji ZX, Sun QS, Xia DS. A modified possibilistic fuzzy C-means clustering algorithm for bias field estimation and segmentation of brain MR image. *Comput Med Imaging Graph* 2011;**35**:383–97
20. Sucharitha M, Geetha KP. Brain tissue segmentation using fuzzy clustering techniques. *Technol Health Care* 2015;**23**:571–80
21. Babu KR, Nagajaneyulu PV, Prasad KS. Brain tumor segmentation of T1w MRI images based on clustering using dimensionality reduction random projection technique. *Curr Med Imaging* 2021;**17**:331–41

22. Blessy SA, Sulochana CH. Performance analysis of unsupervised optimal fuzzy clustering algorithm for MRI brain tumor segmentation. *Technol Health Care* 2015;**23**:23–35
23. Liu L, Kuang L, Ji Y. Multimodal MRI brain tumor image segmentation using sparse subspace clustering algorithm. *Comput Math Methods Med* 2020;**2020**:8620403
24. Wang T, Cheng I, Basu A. Fully automatic brain tumor segmentation using a normalized Gaussian Bayesian classifier and 3D fluid vector flow. In: Proceedings of the 2010 IEEE international conference on image processing, Hong Kong, China, 26–29 September 2010. New York: IEEE
25. Chaddad A. Automated feature extraction in brain tumor by magnetic resonance imaging using Gaussian mixture models. *J Biomed Imag* 2015;**2015**:8
26. Xia Y, Ji Z, Zhang Y. Brain MRI image segmentation based on learning local variational Gaussian mixture models. *Neurocomputing* 2016;**204**:189–97
27. Byale H, Lingaraju G, Sivasubramanian S. Automatic segmentation and classification of brain tumor using machine learning techniques. *Int J Appl Eng Res* 2018;**13**:11686–92
28. Freire PG, Ferrari RJ. Automatic iterative segmentation of multiple sclerosis lesions using student's t mixture models and probabilistic anatomical atlases in FLAIR images. *Comput Biol Med* 2016;**73**:10–23
29. Ji Z, Xia Y, Sun Q, Chen Q, Xia D, Feng DD. Fuzzy local Gaussian mixture model for brain MR image segmentation. *IEEE T Inf Technol Biomed* 2012;**16**:339–47
30. Song Y, Ji Z, Sun Q. An extension Gaussian mixture model for brain MRI segmentation. In: *Proceedings of the 2014 36th annual international conference of the IEEE engineering in medicine and biology society*, Chicago, IL, 26–30 August 2014. New York: IEEE
31. Pravitasari A, Qonita SF, Iriawan N, Irhamah, Fithriasari F, Purnami SW, Ferriastuti W. MRI-based brain tumor segmentation using Gaussian and hybrid Gaussian mixture model-spatially variant finite mixture model with expectation-maximization algorithm. *Malay J Math Sci* 2020;**14**:77–93
32. Chen Y, Zhang H, Zheng Y, Jeon B, Jonathan Wu QM. An improved anisotropic hierarchical fuzzy C-means method based on multivariate student t-distribution for brain MRI segmentation. *Patter Recogn* 2016;**60**:778–92
33. Alqazzaz S, Sun X, Nokes LD, Yang H, Yang Y, Xu R, Zhang Y, Yang X. Combined features in region of interest for brain tumor segmentation. *J Digit Imaging* 2022;**35**:938–46
34. Chen G, Li Q, Shi F, Rekik I, Pan Z. RFDCR: automated brain lesion segmentation using cascaded random forests with dense conditional random fields. *NeuroImage* 2020;**211**:116620
35. Sun L, Zhang S, Chen H, Luo L. Brain tumor segmentation and survival prediction using multimodal MRI scans with deep learning. *Front Neurosci* 2019;**13**:810
36. Ayachi R, Ben Amor N.Brain tumor segmentation using support vector machines. In: *Symbolic and quantitative approaches to reasoning with uncertainty: 10th European conference (ECSQARU 2009)*, Verona, 1–3 July 2009. Cham: Springer
37. Nandpuru HB, Salankar S, Bora V. MRI brain cancer classification using support vector machine. In: *2014 IEEE students' conference on electrical, electronics and computer science*, Bhopal, India, 1–2 March 2014. New York: IEEE
38. Fung G, Mangasarian OL. Proximal support vector machine classifiers. In: *Proceedings of the seventh ACM SIGKDD international conference on knowledge discovery and data mining*, San Francisco, CA, 26–29 August 2001. New York: ACM
39. Vaishnavee K, Amshakala K. An automated MRI brain image segmentation and tumor detection using SOM-clustering and Proximal Support Vector Machine classifier. In: *2015 IEEE international conference on engineering and technology (ICETECH)*, Coimbatore, India, 20 March 2015. New York: IEEE
40. Khemchandani R, Chandra S. Twin support vector machines for pattern classification. *IEEE T Pattern Anal Mach Intell* 2007;**29**:905–10
41. Sahli H, Ben Slama A, Zeraii A, Labidi S, Sayadi M. ResNet-SVM: fusion based glioblastoma tumor segmentation and classification. *J X-ray Sci Technol* 2022;**31**:27–48
42. Vadhnani S, Singh N. Brain tumor segmentation and classification in MRI using SVM and its variants: a survey. *Multim Tools Appl* 2022;**81**:31631–56
43. Tang W, Chen J, Wang Z, Xie H, Hong H. Deep learning for predicting toxicity of chemicals: a mini review. *J Environ Sci Health C Environ Carcinog Ecotoxicol Rev* 2018;**36**:252–71
44. Guo W, Liu J, Dong F, Chen R, Das J, Ge W, Xu X, Hong H. Deep learning models for predicting gas adsorption capacity of nanomaterials. *Nanomaterials* 2022;**12**:3376
45. Sahraeian SME, Fang LT, Karagiannis K, Moos M, Smith S, Santana-Quintero L, Xiao C, Colgan M, Hong H, Mohiyuddin M, Xiao W. Achieving robust somatic mutation detection with deep learning models derived from reference data sets of a cancer sample. *Genome Biology* 2022;**23**:12
46. Pereira S, Pinto A, Alves V, Silva CA. Brain tumor segmentation using convolutional neural networks in MRI images. *IEEE T Med Imaging* 2016;**35**:1240–51
47. Simonyan K, Zisserman A. Very deep convolutional networks for large-scale image recognition. Arxiv Preprint 1409.15562014, https://arxiv.org/abs/1409.1556
48. Nyúl LG, Udupa JK, Zhang X. New variants of a method of MRI scale standardization. *IEEE T Med Imaging* 2000;**19**:143–50
49. AlBadawy EA, Saha A, Mazurowski MA. Deep learning for segmentation of brain tumors: impact of cross-institutional training and testing. *Med Phys* 2018;**45**:1150–8
50. Tong W, Fang H, Xie Q, Hong H, Shi L, Perkins R, Scherf U, Goodsaid F, Frueh F. Gaining confidence on molecular classification through consensus modeling and validation. *Toxicol Mech Methods* 2006;**16**:59–68
51. Ng HW, Doughty SW, Luo H, Ye H, Ge W, Tong W, Hong H. Development and validation of decision forest model for estrogen receptor binding prediction of chemicals using large data sets. *Chem Res Toxicol* 2015;**28**:2343–51
52. Hong H, Harvey BG, Palmese GR, Stanzione JF, Ng HW, Sakkiah S, Tong W, Sadler JM. Experimental data extraction and in silico prediction of the estrogenic activity of renewable replacements for bisphenol A. *Int J Environ Res Publ Health* 2016;**13**:705
53. Gupta S, Gupta M. Deep learning for brain tumor segmentation using magnetic resonance images. In: *2021 IEEE conference on computational intelligence in bioinformatics and computational biology (CIBCB)*, Melbourne, VIC, Australia, 13–15 October 2021. New York: IEEE
54. Qamar S, Jin H, Zheng R, Ahmad P. 3D hyper-dense connected convolutional neural network for brain tumor segmentation. In: *2018 14th international conference on semantics, knowledge and grids (SKG)*, Guangzhou, China, 12–14 September 2018. New York: IEEE
55. Kamnitsas K, Ledig C, Newcombe VFJ, Simpson JP, Kane AD, Menon DK, Rueckert D, Glocker B. Efficient multi-scale 3D CNN with fully connected CRF for accurate brain lesion segmentation. *Med Image Anal* 2017;**36**:61–78
56. Zhao X, Wu Y, Song G, Li Z, Fan Y, Zhang Y. Brain tumor segmentation using a fully convolutional neural network with conditional random fields. In: *Brainlesion: glioma, multiple sclerosis, stroke and traumatic brain injuries: second international workshop, BrainLes 2016, with the challenges on BRATS, ISLES and mTOP 2016, held in conjunction with MICCAI 2016*, Athens, 17 October 2016. Cham: Springer
57. Chen L, Wu Y, DSouza AM, Abidin AZ, Wismüller A, Xu C. MRI tumor segmentation with densely connected 3D CNN. In: *Medical imaging 2018: image processing*, Houston, TX, 2 March 2018. Bellingham, WA: SPIE
58. Shaikh M, Anand G, Acharya G, Amrutkar A, Alex V, Krishnamurthi G. Brain tumor segmentation using dense fully convolutional neural network. In: *Brainlesion: glioma, multiple sclerosis, stroke and traumatic brain injuries: third international workshop, BrainLes 2017, held in conjunction with MICCAI 2017*, Quebec City, QC, Canada, 14 September 2017, Cham: Springer
59. Choromanska A, Henaff M, Mathieu M, Ben Arous G, LeCun Y. The loss surfaces of multilayer networks. In: *Artificial intelligence and statistics*, 2015, https://arxiv.org/abs/1412.0233

60. Krähenbühl P, Koltun V. Efficient inference in fully connected crfs with gaussian edge potentials. *Adv Neur Inform Process Syst* 2011;**24**:109–117
61. Wang G, Li W, Ourselin S, Vercauteren T. Automatic brain tumor segmentation using cascaded anisotropic convolutional neural networks. In: *Brainlesion: glioma, multiple sclerosis, stroke and traumatic brain injuries: third international workshop, BrainLes 2017, held in conjunction with MICCAI 2017*, Quebec City, QC, Canada, 14 September 2017. Cham: Springer
62. Christ PF, Elshaer MEA, Ettlinger F, Tatavarty S, Bickel M, Bilic P, Rempfler M, Armbruster M, Hofmann F, D'Anastasi M, Sommer WH, Ahmadi S-A, Menze BH.Automatic liver and lesion segmentation in CT using cascaded fully convolutional neural networks and 3D conditional random fields. In: *International conference on medical image computing and computer-assisted intervention*, Athens, 17–21 October 2016. Cham: Springer
63. Guan X, Ye J, Yang W, Xu X, Jiang W, Lai X. 3D AGSE-VNet: an automatic brain tumor MRI data segmentation framework. *BMC Med Imaging* 2022;**22**:6
64. Hu J, Shen L, Sun G. Squeeze-and-excitation networks. In: Proceedings of the IEEE conference on computer vision and pattern recognition, Salt Lake City, UT, 18–23 June 2018. New York: IEEE
65. Zhang S, Fu H, Yan Y, Zhang Y, Wu Q, Yang M, Tan M, Xu Y. Attention guided network for retinal image segmentation. In: *Medical image computing and computer assisted intervention–MICCAI 2019: 22nd international conference*, Shenzhen, China, 13–17 October 2019. Cham: Springer
66. Milletari F, Navab N, Ahmadi S-A. V-net: fully convolutional neural networks for volumetric medical image segmentation. In: *2016 fourth international conference on 3D vision (3DV)*, Stanford, CA, 25–28 October 2016. New York: IEEE.
67. Zhou J, Ye J, Liang Y, Zhao J, Wu Y, Luo S, Lai X, Wang J. scSE-NL V-Net: a brain tumor automatic segmentation method based on spatial and channel "squeeze-and-excitation" network with non-local block. *Front Neurosci* 2022;**16**:916818
68. Myronenko A. 3D MRI brain tumor segmentation using autoencoder regularization. In: *Brainlesion: glioma, multiple sclerosis, stroke and traumatic brain injuries: 4th international workshop, BrainLes 2018, held in conjunction with MICCAI 2018*, Granada, 16 September 2018. Cham: Springer
69. Zhou C, Chen S, Ding C, Tao D. Learning contextual and attentive information for brain tumor segmentation. In: *Brainlesion: glioma, multiple sclerosis, stroke and traumatic brain injuries: 4th international workshop, BrainLes 2018, held in conjunction with MICCAI 2018*, Granada, 16 September 2018. Cham: Springer
70. McKinley R, Meier R, Wiest R. Ensembles of densely-connected CNNs with label-uncertainty for brain tumor segmentation. In: *Brainlesion: glioma, multiple sclerosis, stroke and traumatic brain injuries: 4th international workshop, BrainLes 2018, held in conjunction with MICCAI 2018* (Revised Selected Papers, Part II 4.2019), Granada, 16 September 2018. Cham: Springer
71. McKinley R, Rebsamen M, Meier R, Wiest R. Triplanar ensemble of 3D-to-2D CNNs with label-uncertainty for brain tumor segmentation. In: *Brainlesion: glioma, multiple sclerosis, stroke and traumatic brain injuries: 5th international workshop, BrainLes 2019, held in conjunction with MICCAI 2019* (revised selected papers, part I 5.2020.), Shenzhen, China, 17 October 2019. Cham: Springer
72. Zhao Y-X, Zhang Y-M, Liu C-L. Bag of tricks for 3D MRI brain tumor segmentation. In: *Brainlesion: glioma, multiple sclerosis, stroke and traumatic brain injuries: 5th international workshop, BrainLes 2019, held in conjunction with MICCAI 2019* (revised selected papers, part I 5.2020), Shenzhen, China, 17 October 2019. Cham: Springer
73. Ronneberger O, Fischer P, Brox T. U- Net: convolutional networks for biomedical image segmentation. In: *Medical image computing and computer-assisted intervention–MICCAI 2015: 18th international conference (proceedings, part III 18.2015)*, Munich, 5–9 October 2015. Cham: Springer
74. Long J, Shelhamer E, Darrell T. Fully convolutional networks for semantic segmentation. In: *Proceedings of the IEEE conference on computer vision and pattern recognition*, 2015, https://www.cv-foundation.org/openaccess/content_cvpr_2015/papers/Long_Fully_Convolutional_Networks_2015_CVPR_paper.pdf
75. Dong H, Yang G, Liu F, Mo Y, Guo Y. Automatic brain tumor detection | segmentation using U-Net based fully convolutional networks. In: *Medical image understanding and analysis: 21st annual conference, MIUA 2017*, Edinburgh, 11–13 July 2017. Cham: Springer
76. Yang T, Song J. An automatic brain tumor image segmentation method based on the U-Net. In: *2018 IEEE 4th international conference on computer and communications (ICCC)*, Chengdu, China, 7–10 December 2018. New York: IEEE
77. Rehman MU, Cho SB, Kim JH, Chong KT. Bu-net: brain tumor segmentation using modified U-Net architecture. *Electronics* 2020;**9**:2203
78. Kermi A, Mahmoudi I, Khadir MT. Deep convolutional neural networks using U-Net for automatic brain tumor segmentation in multimodal MRI volumes. In: *Brainlesion: glioma, multiple sclerosis, stroke and traumatic brain injuries: 4th international workshop, BrainLes 2018, held in conjunction with MICCAI 2018 (revised selected papers, part II 4.2019.)*, Granada, 16 September 2018. Cham: Springer
79. Badrinarayanan V, Kendall A, Cipolla R. Segnet: a deep convolutional encoder-decoder architecture for image segmentation. *IEEE T Pattern Anal Mach Intell* 2017;**39**:2481–95
80. Li H, Li A, Wang M. A novel end-to-end brain tumor segmentation method using improved fully convolutional networks. *Comput Biol Med* 2019;**108**:150–60
81. Çiçek Ö, Abdulkadir A, Lienkamp SS, Brox T, Ronneberger O. 3D U-Net: learning dense volumetric segmentation from sparse annotation. In: *Medical image computing and computer-assisted intervention–MICCAI 2016: 19th international conference (proceedings, part II 19.2016)*, Athens, 17–21 October 2016. Cham: Springer
82. Albiol A, Albiol A, Albiol F. Extending 2D deep learning architectures to 3D image segmentation problems. In: *International MICCAI brainlesion workshop*, 2018. Springer, https://link.springer.com/chapter/10.1007/978-3-030-11726-9_7
83. Chen W, Peng S, Sun J, Qiao X. S3D-UNet: separable 3D U-Net for brain tumor segmentation. In: *Brainlesion: glioma, multiple sclerosis, stroke and traumatic brain injuries: 4th international workshop, BrainLes 2018, held in conjunction with MICCAI 2018 (revised selected papers, part II 4.2019)*, Granada, 16 September 2018. Cham: Springer
84. Wang G, Li W, Ourselin S, Vercauteren T. Automatic brain tumor segmentation using convolutional neural networks with test-time augmentation. In: Brainlesion: glioma, multiple sclerosis, stroke and traumatic brain injuries: 4th international workshop, BrainLes 2018, held in conjunction with MICCAI 2018 (revised selected papers, part II 4.2019), Granada, 16 September 2018. Cham: Springer
85. Hu K, Gan Q, Zhang Y, Deng S, Xiao F, Huang W, Cao C, Gao X. Brain tumor segmentation using multi-cascaded convolutional neural networks and conditional random field. *IEEE Access* 2019;**7**:92615–29
86. Ghosh S, Chaki A, Santosh KC. Improved U-Net architecture with VGG-16 for brain tumor segmentation. *Phys Eng Sci Med* 2021;**44**:703–12
87. Mazurowski MA, Clark K, Czarnek NM, Shamsesfandabadi P, Peters KB, Saha A. Radiogenomics of lower-grade glioma: algorithmically-assessed tumor shape is associated with tumor genomic subtypes and patient outcomes in a multi-institutional study with The Cancer Genome Atlas data. *J Neurooncol* 2017;**133**:27–35
88. Wibowo MSW, Anggraeni W, Purnomo MH. Automatic brain tumor segmentation using U-Net 2D. In: *2022 international seminar on intelligent technology and its applications (ISITIA)*, Surabaya, Indonesia, 20–21 July 2022. New York: IEEE
89. He K, Zhang X, Ren S, Sun J. Deep residual learning for image recognition. In: *Proceedings of the IEEE conference on computer vision and pattern recognition*, Las Vegas, NV, 27–30 June 2016. New York: IEEE
90. He K, Zhang X, Ren S, Sun J. Identity mappings in deep residual networks. In: *Computer vision–ECCV 2016: 14th European conference (proceedings, part IV 14.2016)*, Amsterdam, 11–14 October 2016. Cham: Springer
91. Goodfellow I, Bengio Y, Courville A. *Deep learning*. Cambridge, MA: MIT Press, 2016

92. Sudre CH, Li W, Vercauteren T, Ourselin S, Cardoso MJ. Generalised dice overlap as a deep learning loss function for highly unbalanced segmentations. In: *Deep learning in medical image analysis and multimodal learning for clinical decision support: third international workshop, DLMIA 2017, and 7th international workshop, ML-CDS 2017, held in conjunction with MICCAI 2017*, Québec City, QC, Canada, 14 September 2017. Cham: Springer
93. Zhang J, Lv X, Zhang H, Liu B. AResU-Net: attention residual U-Net for brain tumor segmentation. *Symmetry* 2020;**12**:721
94. Isensee F, Kickingereder P, Wick W, Bendszus M, Maier-Hein KH. Brain tumor segmentation and radiomics survival prediction: contribution to the BRaTS 2017 challenge. In: *Brainlesion: glioma, multiple sclerosis, stroke and traumatic brain injuries: third international workshop, BrainLes 2017, held in conjunction with MICCAI 2017 (revised selected papers 3.2018)*, Quebec City, QC, Canada, 14 September 2017. Cham: Springer
95. Isensee F, Kickingereder P, Wick W, Bendszus M, Maier-Hein KH. No new-net. In: *Brainlesion: glioma, multiple sclerosis, stroke and traumatic brain injuries: 4th international workshop, BrainLes 2018, held in conjunction with MICCAI 2018 (revised selected papers, part II 4.2019)*, Granada, 16 September 2018. Cham: Springer
96. Mehta R, Arbel T. 3D U-Net for brain tumour segmentation. In: *Brainlesion: glioma, multiple sclerosis, stroke and traumatic brain injuries: 4th international workshop, BrainLes 2018, held in conjunction with MICCAI 2018 (revised selected papers, part II 4.2019)*, Granada, 16 September 2018. Cham: Springer
97. Ulyanov D, Vedaldi A, Lempitsky V. Instance normalization: the missing ingredient for fast stylization. arXiv preprintarXiv:1607.08022, 2016, https://arxiv.org/abs/1607.08022
98. Srivastava N, Hinton G, Krizhevsky A, Sutskever I, Salakhutdinov R. Dropout: a simple way to prevent neural networks from overfitting. *J Mach Learn Res* 2014;**15**:1929–58
99. Jiang Z, Liu M, Tao D. Two-stage cascaded U-Net: 1st place solution to BRaTS challenge 2019 segmentation task. In: *Brainlesion: glioma, multiple sclerosis, stroke and traumatic brain injuries: 5th international workshop, BrainLes 2019, held in conjunction with MICCAI 2019 (revised selected papers, part I 5.2020)*, Shenzhen, China, 17 October 2019, China: Springer
100. Wang Y, Zhang Y, Hou F, Liu Y, Tian J, Zhong C, Zhang Y, He Z. Modality-pairing learning for brain tumor segmentation. In: *Brainlesion: glioma, multiple sclerosis, stroke and traumatic brain injuries: 6th international workshop, BrainLes 2020, held in conjunction with MICCAI 2020 (revised selected papers, part I 6.2021)*, Lima, Peru, 4 October 2020. Cham: Springer
101. Yuan Y. Automatic brain tumor segmentation with scale attention network. In: *Brainlesion: glioma, multiple sclerosis, stroke and traumatic brain injuries: 6th international workshop, BrainLes 2020, held in conjunction with MICCAI 2020 (revised selected papers, part I 6.2021)*, Lima, Peru, 4 October 2020. Cham: Springer
102. Yuan Y. Evaluating scale attention network for automatic brain tumor segmentation with large multi-parametric MRI database. In: *Brainlesion: glioma, multiple sclerosis, stroke and traumatic brain injuries: 7th international workshop, BrainLes 2021, held in conjunction with MICCAI 2021 (revised selected papers, part II.2022)*, Virtual event, 27 September 2021. Cham: Springer
103. Xie S, Sun C, Huan J, Tu Z, Murphy K. Rethinking spatiotemporal feature learning for video understanding. *Arxiv Preprint* 1712;**0485120171**. https://www.arxiv-vanity.com/papers/1712.04851/#:~:text=In%20more%20detail%2C%20our%20methodpurely%20on%20the%20temporal%20axis.
104. Cao Y, Zhou W, Zang M, An D, Feng Y, Yu B. MBANet: a 3D convolutional neural network with multi-branch attention for brain tumor segmentation from MRI images. *Biomed Sign Process Contr* 2023;**80**:104296
105. Kao P-Y, Ngo T, Zhang A, Chen JW, Manjunath BS. Brain tumor segmentation and tractographic feature extraction from structural MR images for overall survival prediction. In: *Brainlesion: glioma, multiple sclerosis, stroke and traumatic brain injuries: 4th international workshop, BrainLes 2018, held in conjunction with MICCAI 2018 (revised selected papers, part II 4.2019)*, Granada, 16 September 2018. Cham: Springer
106. Zhou T, Ruan S, Vera P, Canu S. A Tri-Attention fusion guided multi-modal segmentation network. *Pattern Recogn* 2022;**124**:108417
107. Sheng N, Liu D, Zhang J, Che C, Zhang J. Second-order ResU-Net for automatic MRI brain tumor segmentation. *Math Biosci Eng* 2021;**18**:4943–60
108. Xue Y, Xie M, Farhat FG, Boukrina O, Barrett AM, Binder JR, Roshan UW, Graves WW. A multi-path decoder network for brain tumor segmentation. In: *Brainlesion: glioma, multiple sclerosis, stroke and traumatic brain injuries: 5th international workshop, BrainLes 2019, held in conjunction with MICCAI 2019 (revised selected papers, part II 5.2020)*, Shenzhen, China, 17 October 2019. Cham: Springer.
109. Isensee F, Jaeger PF, Kohl SAA, Petersen J, Maier-Hein KH. nnU-Net: a self-configuring method for deep learning-based biomedical image segmentation. *Nat Methods* 2021;**18**:203–11
110. Isensee F, Jaeger PF, Full PM, Vollmuth P, Maier-Hein KH. nnU-Net for brain tumor segmentation. In: *Brainlesion: glioma, multiple sclerosis, stroke and traumatic brain injuries: 6th international workshop, BrainLes 2020, held in conjunction with MICCAI 2020 (revised selected papers, part II 6.2021)*, Lima, Peru, 4 October 2020. Cham: Springer
111. Luu HM, Park S-H. Extending nn-UNet for brain tumor segmentation. In: *Brainlesion: glioma, multiple sclerosis, stroke and traumatic brain injuries: 7th international workshop, BrainLes 2021, held in conjunction with MICCAI 2021 (revised selected papers, part II.2022)*, Virtual event, 27 September 2021. Cham: Springer
112. Aboelenein NM, Songhao P, Koubaa A, Noor A, Afifi A. HTTU-net: hybrid two track U-Net for automatic brain tumor segmentation. *IEEE Access* 2020;**8**:101406–15
113. Ibtehaz N, Rahman MS. MultiResUNet: rethinking the U-Net architecture for multimodal biomedical image segmentation. *Neural Netw* 2020;**121**:74–87
114. Sahayam S, Nenavath R, Jayaraman U, Prakash S. Brain tumor segmentation using a hybrid multi resolution U-Net with residual dual attention and deep supervision on MR images. *Biomed Sign Process Contr* 2022;**78**:103939
115. Karimi D, Salcudean SE. Reducing the hausdorff distance in medical image segmentation with convolutional neural networks. *IEEE T Med Imaging* 2019;**39**:499–513
116. Kumar P, Nagar P, Arora C, Gupta A. U-segnet: fully convolutional neural network based automated brain tissue segmentation tool. In: *2018 25th IEEE international conference on image processing (ICIP)*, Athens, 7–10 October 2018. New York: IEEE
117. Kong X, Sun G, Wu Q, Liu J, Lin F. Hybrid pyramid U-Net model for brain tumor segmentation. In: *Intelligent information processing IX: 10th IFIP TC 12 international conference, IIP 2018*, Nanning, China, 19–22 October 2018. Cham: Springer
118. Ioffe S, Szegedy C. Batch normalization: accelerating deep network training by reducing internal covariate shift. In: *International conference on machine learning*, 2015, https://arxiv.org/abs/1502.03167
119. Kamnitsas K, Bai W, Ferrante E, McDonagh S, Sinclair M, Pawlowski N, Rajchl M, Lee M, Kainz B, Rueckert D, Glocker B. Ensembles of multiple models and architectures for robust brain tumour segmentation. In: *Brainlesion: glioma, multiple sclerosis, stroke and traumatic brain tnjuries: third international workshop, BrainLes 2017, held in conjunction with MICCAI 2017 (revised selected papers 3.2018)*, Quebec City, QC, Canada, 14 September 2017. Cham: Springer
120. Jia H, Cai W, Huang H, Xia Y. H2NF-Net for brain tumor segmentation using multimodal MR imaging: 2nd place solution to BraTS challenge 2020 segmentation task. In: *Brainlesion: glioma, multiple sclerosis, stroke and traumatic brain injuries: 6th international workshop, BrainLes 2020, held in conjunction with MICCAI 2020 (revised selected papers, part II 6.2021)*, Lima, Peru, 4 October 2020. Cham: Springer
121. Praveen G, Agrawal A. Hybrid approach for brain tumor detection and classification in magnetic resonance images. In: *2015 communication,*

control and intelligent systems (CCIS), Mathura, India, 7–8 November 2015. New York: IEEE
122. Saha BN, Ray N, Greiner R, Murtha A, Zhang H. Quick detection of brain tumors and edemas: a bounding box method using symmetry. *Comput Med Imaging Graph* 2012;**36**:95–107
123. Deepa S, Devi BA. Artificial neural networks design for classification of brain tumour. In: *2012 international conference on computer communication and informatics*, Coimbatore, India, 10–12 January 2012. New York: IEEE
124. Ghanavati S, Li J, Liu T, Babyn PS, Doda W, Lampropoulos G. Automatic brain tumor detection in magnetic resonance images. In: *2012 9th IEEE international symposium on biomedical imaging (ISBI)*, Barcelona, 2–5 May 2012. New York: IEEE
125. Iftekharuddin K, Zheng J, Islam MA, Ogg RJ, Lanningham F. Brain tumor detection in MRI: technique and statistical validation. In: *2006 Fortieth Asilomar conference on signals, systems and computers*, Pacific Grove, CA, 29 October–1 November 2006. New York: IEEE
126. Preetha R, Suresh G. Performance analysis of fuzzy C means algorithm in automated detection of brain tumor. In: *2014 world congress on computing and communication technologies*, Trichirappalli, India, 27 February–1 March 2014. New York: IEEE
127. Megersa Y, Alemu G. Brain tumor detection and segmentation using hybrid intelligent algorithms. In: *AFRICON 2015*, Addis Ababa, Ethiopia, 14–17 September 2015. New York: IEEE
128. Kazemi FM, Akbarzadeh-T M-R, Rahati S, Rajabi H. Fast image segmentation using C-means based Fuzzy Hopfield neural network. In: *2008 Canadian conference on electrical and computer engineering*, Niagara Falls, ON, 4–7 May 2008. New York: IEEE
129. Sreedhanya S, Pawar CS. An automatic brain tumor detection and segmentation using hybrid method. *Int J Appl Inform Syst* 2017;**11**: 6–11
130. Abdel-Maksoud E, Elmogy M, Al-Awadi R. Brain tumor segmentation based on a hybrid clustering technique. *Egypt Inform J* 2015;**16**:71–81
131. Cengil E, Cinar A. . A deep learning based approach to lung cancer identification. In: *2018 international conference on artificial intelligence and data processing (IDAP)*, Malatya, 28–30 September 2018. New York: IEEE